HYDROLOGICAL PROCESSES
Hydrol. Process. (2012)
Published online in Wiley Online Library
(wileyonlinelibrary.com) DOI: 10.1002/hyp.9240

The hydrogeomorphic influences on alluvial gully erosion along the Mitchell River fluvial megafan

J. G. Shellberg,* A. P. Brooks, J. Spencer and D. Ward
Australian Rivers Institute, Griffith University, Nathan, Queensland 4111, Australia

Abstract:

Hydrogeomorphic processes influencing alluvial gully erosion were evaluated at multiple spatial and temporal scales across the Mitchell River fluvial megafan in tropical Queensland, Australia. Longitudinal changes in floodplain inundation were quantified using river gauge data, local stage recorders and HEC-RAS modelling based on LiDAR topographic data. Intra- and interannual gully scarp retreat rates were measured using daily time-lapse photographs and annual GPS surveys. Erosion was analysed in response to different water sources and associated erosion processes across the floodplain perirheic zone, including direct rainfall, infiltration-excess runoff, soil-water seepage, river backwater and overbank flood inundation. The frequency of river flood inundation of alluvial gullies changed longitudinally according to river incision and confinement. Near the top of the megafan, flood water was contained within the macrochannel up to the 100-year recurrence interval, but river backwater still partially inundated adjacent gullies eroding into Pleistocene alluvium. In downstream Holocene floodplains, inundation of alluvial gullies occurred beyond the 2- to 5-year recurrence interval and contributed significantly to total annual erosion. However, most gully scarp retreat at all sites was driven by direct rainfall and infiltration-excess runoff, with the 24-h rainfall total being the most predictive variable. The remaining variability can be explained by seasonal vegetative conditions, complex cycles of soil wetting and drying, tension crack development, near-surface pore-water pressure, soil block undermining from spalling and overland flow, and soil property heterogeneity. Implications for grazing management impacts on soil surface and perennial grass conditions include effects on direct rainfall erosion, water infiltration, runoff volume, water concentration along tracks, and the resistance of highly dispersible soils to gully initiation or propagation under intense tropical rainfall. Copyright © 2012 John Wiley & Sons, Ltd.

KEY WORDS alluvial gully erosion; floodplain connectivity; rainfall erosion; infiltration-excess runoff; erosion resistance; grazing management

Received 11 July 2011; Accepted 2 February 2012

INTRODUCTION

Alluvial gullies are incisional features entrenched into alluvium typically not previously incised since initial deposition. They are often located adjacent to large rivers or floodplain water bodies (Brooks *et al*., 2009) and have inconspicuous floodplain catchment areas that are difficult to delineate and infer fluvial processes from (i.e. slope–area thresholds, rainfall–runoff response). Alluvial gullies have been inconsistently described in the literature as valley-bottom gullies, bank gullies, ravines and alluvial breakaways from locations around the world (USA: Brice, 1966; Piest *et al*., 1975; Thomas *et al*., 2004; Australia: Simpson and Doutch, 1977; Condon, 1986; Pickup, 1991; Pringle *et al*., 2006; Brooks *et al*., 2008; 2009, McCloskey, 2010; Europe: Poesen, 1993; Vandekerckhove *et al*., 2000, 2001, 2003; Africa: Oostwoud Wijdenes and Bryan, 2001; India: Singh and Dubey, 2000; Yadav and Bhushan, 2002). Alluvial gully initiation and evolution can span large spatial and temporal scales in floodplain environments, from small anthropogenically enhanced alluvial gullies (e.g. Vandekerckhove *et al*., 2001, 2003) to large alluvial gully tributaries cut into floodplains during low sea level stands and inundated by backwater during high stands (e.g. Mertes and Dunne, 2008; Parker *et al*., 2008).

Only a few studies have quantified the hydrogeomorphic mechanisms responsible for the propagation or initiation of alluvial gully erosion. 'Valley-bottom' gullies in Iowa are eroded by both direct rainfall–runoff and groundwater seepage enhancing mass failure (Piest *et al*., 1975; Thomas *et al*., 2004). In Kenya, Oostwoud Wijdenes and Bryan (2001) observed that rainfall–runoff processes dominated erosion in a 'catchment controlled' alluvial gully but did not quantify hydrologic processes at 'base-level controlled' gullies along floodplain rivers. Alluvial 'bank gullies' in Spain are driven by rainfall–runoff processes enhanced by agriculture activities (Oostwoud Wijdenes *et al*., 2000; Wijdenes *et al*., 2000; Vandekerckhove *et al*., 2000, 2001, 2003). In India, alluvial ravines and gullies are influenced by surface water runoff from agricultural land (Haigh, 1998; Yadav and Bhushan, 2002), tunnel erosion and groundwater seepage (Sharma, 1987) and river backwater during flood (Singh and Dubey, 2000; Yadav and Bhushan, 2002). For alluvial gully erosion in northern Australia, preliminary observations by Brooks *et al*. (2009) suggested that hydrological mechanisms influencing gully initiation or propagation could span the full continuum of surface and subsurface erosion models (Horton, 1933; Kirkby and

*Correspondence to: J. G. Shellberg, Building N13, 1.19A, 170 Kessels Road, Nathan, Queensland 4111, Australia.
E-mail: j.shellberg@griffith.edu.au

Chorley, 1967; Dunne and Black, 1970; DeVries, 1976; Kirkby, 1988; Bryan and Jones, 1997), in addition to erosion induced by river backwater and overbank flooding. If predictive models of gully initiation and evolution are to be developed and incorporated into sediment budgets, it is imperative that we understand the relative importance of the various hydrological drivers and associated erosion processes of alluvial gully erosion.

Research objectives

The aim of this research was to quantify hydrogeomorphic processes that influence alluvial gully erosion along the Mitchell River fluvial megafan in northern Australia. The specific objectives were (i) to quantify longitudinal changes in inundation hydrology and river connectivity with adjacent floodplains and alluvial gullies, (ii) to quantify the intra-annual hydrology and erosion dynamics of alluvial gullies as influenced by local rainfall–runoff and floodplain inundation and (iii) to develop a conceptual model of how different water sources and associated erosion processes across the floodplain perirheic zone (*sensu* Mertes, 1997) influence the initiation or propagation of alluvial gullies. A hierarchical approach was taken, which addressed geomorphic structures and hydrogeomorphic processes at multiple spatial and temporal scales (Poole, 2002), from the entire fluvial megafan, to river segments, to large gully-complexes and to individual head-cut lobes within a gully.

REGIONAL SETTING

Mitchell fluvial megafan and alluvial gullying

The study area was focused within the Mitchell River fluvial megafan, a 31 000-km^2 area of nested fluvial fans and river floodplains concentrated in the lower half of the Mitchell River catchment (71 630 km^2; Figure 1; Brooks *et al.*, 2009). The evolution of the megafan from the Pliocene to Holocene (Grimes and Doutch, 1978) has developed a unique assemblage of geomorphic units and process zones that vary both longitudinally and transversely across the megafan (Galloway *et al.*, 1970). River incision into the megafan and backfilled floodplain units upstream has shifted the hydrologic apex from near the Lynd River confluence (Pleistocene apex) to below the Palmer River confluence (Holocene apex of the Mitchell fandelta) (Figures 1 and 2). The increase in local relative relief over geologic time has set up the potential energy needed for a secondary cycle of erosion (*sensu* Pickup, 1985), enhancing the potential for alluvial gully erosion that is

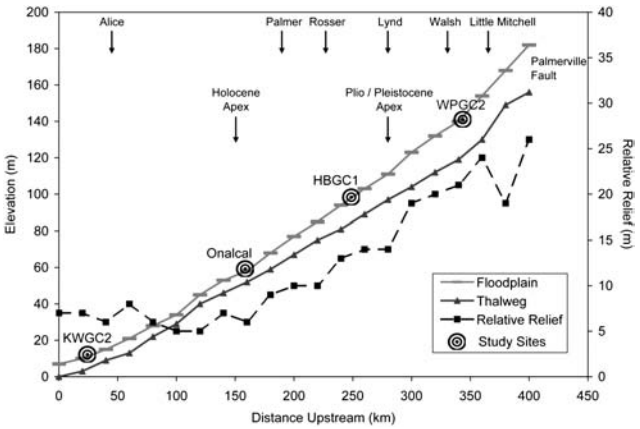

Figure 2. Longitudinal profile of the Mitchell River thalweg and adjacent high-floodplain surface derived from cross sections using the 1-s Shuttle Radar Topography Mission DEM. Major study sites from upstream to downstream are Wrotham Park (WPGC2), Highbury (HBGC1), Onalcal Bar (Onalcal) and Sandy Creek (KWGC2). Upstream river tributary locations and current and past megafan apexes are also noted.

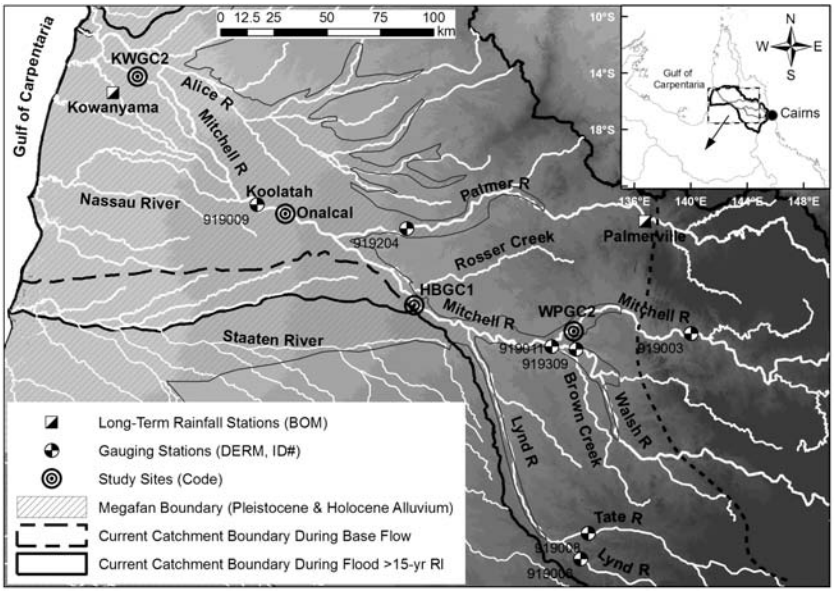

Figure 1. Map of the lower Mitchell catchment, fluvial megafan boundary (Pleistocene and Holocene alluvium, Grimes and Doutch 1978), study sites and gauging stations. The grey scale background represents 30-m elevation bands derived from the 1-s Shuttle Radar Topography Mission. Major study sites from upstream to downstream are Wrotham Park (WPGC2), Highbury (HBGC1), Onalcal Bar (Onalcal) and Sandy Creek (KWGC2). The dashed line is the Palmerville fault that marks the transition from bedrock upstream to alluvium downstream.

DOI: 10.1002/hyp

widespread (>129 km^2) along the lower Mitchell River (Brooks *et al*., 2009). These alluvial gullies are an effective and dominant source of sediment in the Mitchell catchment, producing cumulatively >3.5 Mt/year (Brooks *et al*., 2008; Rustomji *et al*., 2010; Shellberg, 2011).

Climate

The monsoonal, wet–dry tropical climate of the Mitchell catchment (Stewart, 1993; Ward *et al*., 2011) is important from both surface soil erosion and floodplain inundation perspectives. The catchment receives >80% of its annual rainfall and river runoff from December to March. Annual rainfall in the lower catchment averages 1015 mm and varies between 500 and 2100 mm (ABOM, 2010). Storm rainfall intensity and erosivity (*R*-factors) are moderately high (Stewart, 1993; Yu, 1998; Lu and Yu, 2002). Potential evapotranspiration is 1700 to 2000 mm per year, whereas actual evapotranspiration is 600 to 900 mm per year (ABOM, 2010). Soils are completely desiccated by the late dry season. Soil moisture also can be partially or fully depleted between storms and synoptic disturbances within the wet season because of high actual evapotranspiration and low infiltration rates into hard-setting, sodic soils.

Land use

The dominant land use across the lower Mitchell catchment is cattle grazing across savanna woodlands and grasslands. During the long dry season, cattle grazing intensity and effects are heavily concentrated along 'waterway frontages' or riparian zones of main rivers and tributaries. Access to in-channel pools and lagoons has allowed for the continuous stocking of cattle near water bodies throughout the year (Tothill *et al*., 1985). Many of the alluvial gullies across the Mitchell megafan initiated post-European settlement during the period when cattle numbers increased significantly from the 1880s onwards (Shellberg *et al*., 2010; Shellberg, 2011). Gully initiation points were located at relatively steep river banks or within unchannelled floodplain hollows, where cattle impacts such as overgrazing and soil disturbance were the greatest.

MATERIALS AND METHOD

Study sites

Alluvial gully erosion study sites and adjacent river reaches were situated at different longitudinal positions down the Mitchell River fluvial megafan (Figures 1 and 2). Three quantitative gully-complex sites at Wrotham Park (WPGC2), Highbury (HBGC1) and Sandy Creek (KWGC2) were selected on the basis of their major differences in relative relief between the river high-floodplain and the adjacent river channel. One additional gully was only qualitatively observed through time at Onalcal Bar near Koolatah (Figure 1) because of the reduced presence and activity of alluvial gullies in this area (Brooks *et al*., 2009). Gully-complex sites were representative of the most common proximally draining alluvial gullies mapped and visited by Brooks *et al.* (2008; 2009), in contrast to distally draining gullies and gullies tributary to creeks and water bodies on the surface of the megafan.

River reach characteristics

At each gully-complex site, a reach of river centred on the gully confluence was selected to investigate geomorphic and hydrologic characteristics and interactions between the gully and the river channel (Table I). The reaches were delineated using airborne light detection and ranging (LiDAR) surveys. These data were used to define the topographic, geomorphic and hydraulic characteristics of the river reach, the adjacent gully-complex and their interactions. The geomorphology of each river reach was unique, but sites were chosen to be representative of major processes zones down the Mitchell megafan.

Gully characteristics

LiDAR data revealed the topographic variability in the proximal gully-complexes and associated floodplains (Figure 3). At all sites, pre-gully floodplain hollows, palaeochannel depressions or other shallow fluvial drainage forms existed on river inset- and high-floodplains, as indicated by remnant and partially dissected floodplain features. Subsequently, a major unprecedented phase of gully incision progressed via head cutting through many of these features, migrating through the riparian zone into the relatively flat river high-floodplains and Eucalyptus woodlands (Shellberg *et al*., 2010; Shellberg, 2011). Alternatively, gully erosion also incised directly into the river high-floodplains at river banks in the absence of any preceding drainage forms (Figure 3; Brooks *et al*., 2009).

The silt and clay soils along river high-floodplains 1 to 2 km from the river are massive, sodic, hard setting, low in organic matter and scald prone (Galloway *et al*., 1970; BRS, 1991). Subtle textural contrasts exist between the coarsest material mid-profile and the finer material above and below, whereas strong chemical contrasts occur down profile (Table II). Because of their sodic nature and exchangeable sodium percentage values >6%, these soils are highly dispersive with a predisposition to erosion (Naidu *et al*., 1995). Their weathered tropical chemistry and cyclic wetting and drying also promote soil mottling and concretion development, which readily produce surface lags of pisoliths of ferricrete and calcrete after permanent oxidation following gullying (Goudie, 1973; Pain and Ollier, 1992).

Water stage and discharge data

Continuous water stage recorders (pressure transducers) were installed along the lower reach of each gully outlet channel to define the inundation hydrology of each main stem river reach and adjacent alluvial gully-complexes (Figure 3). Deployment during water years (October–September) WY 2008 to WY 2010 measured both surface runoff from gully-complexes during low

DOI: 10.1002/hyp

Table I. River reach characteristics at study sites

River reach	Wrotham Park	Highbury	Onalcal Bar	Sandy Creek
Channel type[a]	Planform-controlled, inset-wandering, gravel-bed river	Planform-controlled, low-sinuosity, bar-braided, sand-bed river	Wandering sand-bed river (meandering to braided transition)	Distributary (near tidal interface)
Bed material	Gravel with sand chutes and shale outcrops	Sand/gravel with outcrops of indurated alluvium and sandstone	Sand with minor gravel	Sand with outcrops of indurated alluvium and sandstone
River floodplains	Sand and gravel capped with sand/silt/clay	Sand and indurated alluvium capped with silt/clay	Sand capped with silt/clay	Sand and indurated alluvium capped with silt/clay
Riparian forests	Thalweg: *Melaleuca* spp. River inset-floodplain: *Eucalyptus* spp., *Cryptostegia grandiflora* (exotic), rainforest spp. River high-floodplain: mixed *Eucalyptus* spp. open woodland	Thalweg: *Melaleuca* spp. River inset-floodplain: *Eucalyptus* spp., rainforest spp. River high-floodplain: mixed *Eucalyptus* spp. open woodland	Thalweg: *Melaleuca* spp. River inset-floodplain: *Eucalyptus* spp., *Nauclea orientalis*, *C. grandiflora* (exotic), rainforest spp. River high-floodplain: mixed *Eucalyptus* spp. open woodland	Thalweg: *Melaleuca* spp. River inset-floodplain: *Corypha utan, Melaleuca* spp., *Eucalyptus* spp. River high-floodplain: *Eucalyptus microtheca* and other *Eucalyptus* spp.
Macrochannel width (km)	0.8–1.2	0.6–0.9	1.5–3.0	0.1–0.3
Slope (m/m)	0.0029[b]	0.0014[c]	Average: 0.00037[d] Range: 0.00027–0.00052	~0.0001 (near tidal interface)
LiDAR reach length (km)	1.5	2.0	6.5	1.3
LiDAR total area (km^2)	6.8	5.8	26	1.4
No. Cross sections, extracted from LiDAR	30	52	87	N/A
Composite Manning's n roughness (channel = back-calculated)	Channel: 0.08–0.15 Floodplain: 0.20	Channel: 0.03–0.06 Floodplain: 0.15	Channel: 0.025–0.045 Floodplain: 0.10	N/A
Discharge (Q) estimates from local stage correlations with QDERM gauged Q	Q Mitchell at Gamboola (919011) minus Q Walsh at Trimbles (919309), corrected for basin area differences	Q Mitchell at Koolatah (919009) minus Q Palmer at Drumduff (919204), corrected for basin area differences and 30% water loss	Q Mitchell at Koolatah (919009)	N/A
Flood-frequency (RI) estimates	Average of RI Mitchell at Gamboola (919011) and RI Walsh at Trimbles (919309)	Q at target RI from Mitchell at Gamboola (919011) + Q Tate at Torwood (919008) + Q Lynd at Torwood (919006), corrected for basin area differences	RI Mitchell at Koolatah (919009)	RI Mitchell at Koolatah (919009)

N/A, not available.
[a] Modified from Brennan and Gardiner (2004).
[b] Estimated from LiDAR reach bed slope and measured flood water surface slope(s) at Gamboola gauge (919011).
[c] Estimated from LiDAR reach bed slope.
[d] Measured flood water surface slope (average) from continuous stage gauges 8 km apart.

DOI: 10.1002/hyp

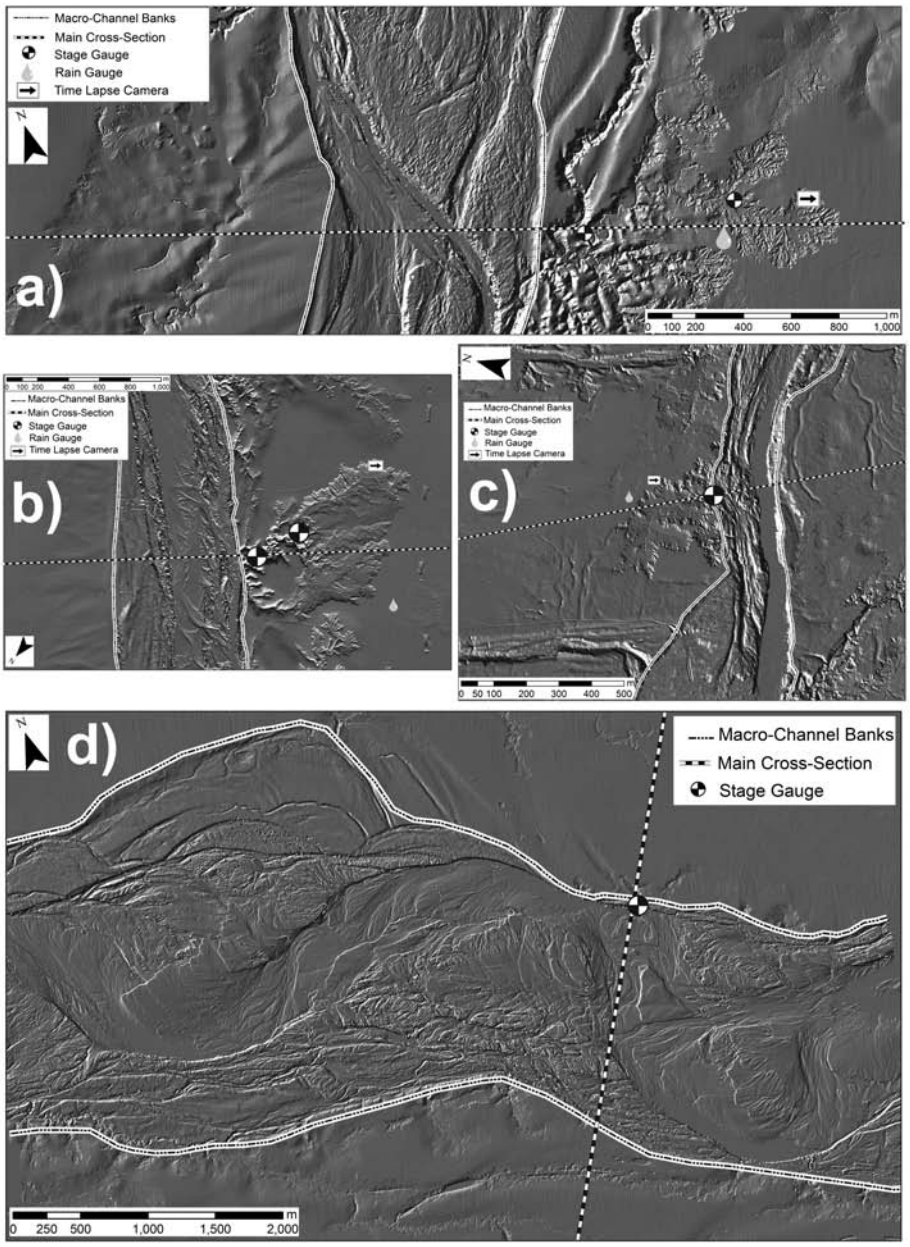

Figure 3. LiDAR hillshade maps of the different alluvial gully-complex sites and adjacent river reaches used for hydraulic analysis: (a) Mitchell River near Wrotham Park (WPGC2), (b) Mitchell River near Highbury (HBGC1), (c) Sandy Creek near Kowanyama (KWGC2) and (d) Mitchell River near Koolatah (Onalcal Bar). Flow direction is from top to bottom for panels a–c and from right to left for panel d. Main cross-sectional data for locations in panels a–d are also displayed in Figure 7.

river stage and river stage and backwater conditions into gully-complexes during flood conditions. At WPGC2 and HBGC1 where the relative relief was greatest, a second set of stage recorders was installed higher in the gully networks to better isolate local rainfall–runoff processes in the absence of anticipated river backwater. Only at the WPGC2 upper gauge was a stage–discharge relationship developed specifically for the gully channel in isolation of backwater effects (Shellberg, 2011).

Instantaneous water stage and discharge data from permanent river gauges in the lower Mitchell catchment (Figure 1; QDERM, 2010) were obtained for their period of record (~1973–2010). These data were used for flood frequency analysis and correlation with stage data collected at alluvial gully sites (i) to estimate river discharge flowing through the study reaches and (ii) to estimate the flood frequency of specific stage and discharge conditions at study reaches.

Flood frequency from gauge records

At river gauge stations, annual peak discharges for the period of record were used to estimate annual flood recurrence intervals (RIs; inverse of exceedance probability) following the log-Pearson type III distribution (USWRC, 1981; Cudworth, 1989). Weighted skew coefficients were calculated from station coefficients and a generalized skew coefficient from 15 regional gauging stations (>20 years of data within ~150 km radius; USWRC, 1981). The fitted log-Pearson type III distribution was as reasonable as any other estimate of the population distribution because the

DOI: 10.1002/hyp

Table II. Gully and soil characteristics at study sites and gully head soil profiles

Gully	WPGC2 (Wrotham Park)	HBGC1 (Highbury)	Onalcal (Onalcal Bar)	KWGC2 (Sandy Creek)
Internal gully area (ha)	7.8	50	1	6
Gully-complex area (ha)	~50	55	1	8
Drainage direction	Proximal 1–2 km from river	Proximal 1–2 km from river	Proximal <1 km from river	Proximal <1 km from river
Soil type at gully head	Sodic, hard setting, silt/clay alluvium, red and yellow earths	Sodic, hard setting, silt/clay alluvium, red and yellow earths	Hard setting, silt/clay alluvium, red and yellow earths	Sodic, hard setting, silt/clay alluvium red, yellow and grey earths
Max depositional age[b]	Pleistocene	Pleistocene	Holocene	Holocene
Median particle size d_{50} (μm)[a]	Profile median: 50 Range: 80 at 1 m depth, finer above and below	N/A	N/A	Profile median: 20 Range: 30 at 0.5 m depth finer above and below
Bulk density (kg/m^3)	Average: 2035 Range: 1800–2200 increasing with depth	Average: 2057 Range: 1950–2100 increasing with depth	N/A	Average: 1859 Range: 1720–1970, peak at 50 cm
Soil conductivity (μS cm^{-1} at 25 C) (1:5 soil/water ratio)	Average: 161 Range: 14–520 increasing with depth	Average: 313 Range: 134–764 increasing with depth	N/A	Average: 718 Range: 25–2700 increasing with depth
pH (1:5 soil/water ratio)	Average: 7.3 Range: 5.0–9.1 increasing with depth	Average: 5.6 Range: 4.5–7.5 increasing with depth	N/A	Average: 6.4 Range: 4.8–7.5 increasing with depth
Exchangeable sodium percentage[c]	Average: 11.2 Range: 5–17 increasing with depth	Average: 45.5 Range: 26–66 increasing with depth	N/A	Average: 5.9 Range: 4–8 increasing with depth

N/A, not available.

[a] Particle size distribution measured using a Coulter multisizer (McTanish *et al.*, 1997).

[b] Upper surface could be younger (Grimes and Doutch, 1978).

[c] Exchangeable sodium percentage = $[(Na^{+1}) / (K^{+1} + Na^{+1} + Ca^{+2} + Mg^{+2})] \times 100$ using units of mEq/100 g. Values >6 represent sodic soils. Methods followed Rayment and Higginson (1992) using a pretreatment for soluble salts (ethanol/glycerol) and cation extraction using ammonium acetate (CH_3COONH_4) at pH 7.

DOI: 10.1002/hyp

annual peak data were hampered by (i) sample size (<40 years), (ii) flood discharge measurement error (±15%–25%) and (iii) rating curve extrapolation for discharge events >10-year RI (Cudworth, 1989).

Discharge and flood frequency correlations

Discharge and flood frequency data at river gauge stations were transferred to study reaches through correlation with local continuous water stage. For different flood events, peak instantaneous discharge values at gauged sites were corrected for gauged tributary inputs and ungauged catchment area and then correlated to peak stage values at study sites, offset in time due to flood wave transmission. At each study reach, stage–discharge curves at low to moderate flood stages measured during the study period were developed. These data were used to calibrate one-dimensional (1D) hydraulic models (HEC-RAS) for each reach (described below), from which the upper portions of the local rating curves were modelled.

Wrotham Park. The peak discharge for specific flood events (<12-year RI) during the study period was estimated at the Wrotham Park reach by subtracting the Walsh River at Trimbles (919309) discharge from the Mitchell River at Gamboola (919011) discharge, corrected for ungauged catchment area differences (Figure 1; Table I). This reach's flood RIs were estimated as the average RI from the same peak flood event at the Gamboola and Trimbles gauges. Flood discharge estimates at targeted RIs (25-, 50- and 100-year RI) were calculated by subtracting the Walsh (919309) from Mitchell (919011) discharge at the target RI, corrected by catchment area. The local-reach water stages of these high magnitude peak discharges and RIs were estimated from HEC-RAS 1D hydraulic modelling.

Highbury. Hydrologic analysis at Highbury was hampered by discontinued data collection at the Lynd gauging stations (919006 and 919008; Figure 1). Therefore, discharge was measured directly at this river reach during river flood (February 2009, peak of 7115 $m^3 \cdot s^{-1}$ at 88.7 m water elevation, Figures 6b and 7b) using both boat mounted current meters (Ott-C31) and an acoustic Doppler current profiler (RD Instruments). These data were used to confirm correlations with the downstream gauges during the study period. Highbury peak discharge was estimated by subtracting Palmer (919204) peak discharge data from Koolatah (919009) discharge, corrected for unmeasured catchment area and 30% channel water loss measured during sequential downriver discharge measurements below bankfull (Figure 1; Table I). This method output was generally comparable with Highbury peak discharge estimates from a basic basin area correction of the upstream Gamboola (919011) peak flood data (Gamboola area 58% of Highbury due to Lynd River; Figure 1).

Flood discharge estimates at targeted RIs (10- and 25-year RI) were calculated by adding the peak discharges from the Mitchell at Gamboola (919011), Tate at Torwood (919008) and Lynd at Torwood (919006) gauges, corrected for unmeasured catchment area. This method avoided issues with excessive water loss at Koolatah during extreme events. It provides a maximum estimate of peak discharge, assuming that Mitchell and Lynd flood peaks arrive at the same time and RI, which might not be unreasonable during the landfall of synoptic-scale tropical cyclones common in this catchment (Nott *et al*., 2007).

Onalcal Bar. Continuous discharge data during the study period were available for the Koolatah gauge (919009) 16 km downstream of the Onalcal Bar reach (Figure 1). Flood peak timing was only slightly offset, and transfer of discharge and flood frequency data was relatively direct (Table I). These data along with local discharge measurements (February 2009) were used to calibrate the HEC-RAS 1D hydraulic model for this reach and estimate water stages for specific discharges and RIs.

Sandy Creek. No discharge estimates were made for the Sandy Creek reach (KWGC2) because it is one of dozens of distributaries fed by the Mitchell River below the Koolatah gauge (919009). Rather, direct correlations were made between peak stage at Sandy Creek and peak stage and RI at the Koolatah gauge. No estimates of flood frequency were made beyond the bankfull stage defined by LiDAR cross sections, as most the landscape becomes inundated beyond this elevation.

Hydraulic modelling

LiDAR topographic data were collected at baseflow conditions (November 2008) and used to create 1 m^2 pixel digital elevation models (DEMs) for each reach (Figure 3). HEC-GeoRAS (Cameron and Ackerman, 2009) was used to extract reach cross sections and estimate other geomorphic parameters (Table I). HEC-RAS models (Brunner, 2010) were calibrated for the study period (excluding Sandy Creek reach) using the previously described stage–discharge correlations. Representative energy slopes were estimated from the LiDAR reach bed slopes, water surface slopes measured at gauging stations during flood and paired water stage recorders 8 km apart at the Onalcal Bar reach (Table I). Spatially uniform channel roughness values within the macrochannel were back-calculated from estimated low and moderate flood discharge values, known water surface elevations and channel geometry data. Dense overbank riparian vegetation areas were visually assigned Manning's *n* roughness values (Chow, 1959). To estimate water surface elevations for larger target RI discharges, we adjusted back-calculated roughness values for the macrochannel for slight increasing trends in roughness with increasing stage as forested inset-floodplains in the river macrochannel became inundated, as supported by empirical trends.

Remote sensing of flood frequency

Remote sensing analysis of floodplain inundation frequency for the lower Mitchell fandelta supplemented the atypical flood frequency curves for the Koolatah (919009) gauge. Moderate Resolution Imaging Spectro-radiometer (MODIS) satellite imagery (2003–2009) was used to estimate the *visual* inundation frequency of different

DOI: 10.1002/hyp

parts of the Mitchell fandelta covering over a dozen flood events not obstructed by cloud cover (Ward *et al.*, 2012, accepted). These data provide minimum inundation frequency estimates due to image availability, 250 m pixel size and mixed spectral signals, masking by dense riparian vegetation cover >30%, and other issues detecting episodic shallow inundation from local rainfall or floods. This minimum inundation frequency was compared with the mapped minimum extent of alluvial gullies (Brooks *et al.*, 2009), and the percentage of alluvial gullies inundated one or more times was estimated.

Gully scarp erosion measurements

Interannual changes in gully scarp location along the total gully perimeter of each site were measured annually between 2007 and 2010 using a differential global positioning system (GPS) within ±50 cm horizontal accuracy (Trimble with Omnistar HP; Brooks *et al.*, 2009). Intra-annual variation in gully scarp erosion was assessed and measured using time-lapse cameras (digital, nonphotogrammetric and small format), which were programmed to take daily photographs at specific index scarp sections (Figure 3). These sections were representative of average conditions across the scarp perimeter. Cameras were operated from WY 2008 to WY 2010. However, camera failure occurred during WY 2008 at WPGC2 and HBGC1, whereas additional data were collected at WPGC2 during WY 2011. Cameras were mounted on stable trees and pointed at an oblique angle at index scarp sections. The digital photographs (2848 × 2136 pixels, ~6 MP) were rectified to each other in a GIS using ground control points. The gully scarp edge was digitized daily after intervals of observable change. Because of the oblique angle, only a relative change in gully area at the scarp edge could be measured, which was calculated as the percentage of daily change divided by the total change over the period of record. To estimate actual planform change, we multiplied the percentage of daily change divided by the total change against the horizontal area change measured during annual GPS surveys. These erosion index data were then compared against daily rainfall metrics, water surface stages and photographic observations of hydrological processes.

Local rainfall and water stage metrics

Continuous rainfall data were collected using automated tipping buckets (0.2 mm) at WPGC2, HBGC1, KWGC2 (Figures 1 and 3) during WY 2008–2010, in addition to WY 2011 at WPGC2. Rainfall metrics were derived from these data to compare with daily changes in scarp erosion documented from time-lapse cameras. These included the 24-, 48- and 72-h total rainfall, daily maximum 30-min rainfall intensity (max I_{30}), daily rainfall erosivity (EI_{30}) and a normalized antecedent precipitation index (NAPI). EI_{30} was calculated as the product of the daily sum of storm kinetic energy (E) times the daily maximum 30-min intensity (I_{30}) (Renard *et al.*, 1997; Yu, 1998). Storms with >12.7 mm (0.5 in) of total rainfall (i.e. effective storms) separated by 6 h of no rain were used to compute daily EI_{30} (Yu, 1998). A 5-day inclusive NAPI (Heggen, 2001) was calculated using daily rainfall totals and two different decay coefficients (k), 0.8 and 0.2. The former is a typical literature value whereas the later was more representative of the rapid decay of rainfall–runoff and soil moisture at alluvial gully sites due to climatic and soil factors.

These rainfall metrics along with daily mean and maximum water stage were analysed as independent variables in a stepwise multiple linear regression model to predict the dependent variable of daily scarp erosion documented from time-lapse cameras. Because of the intercorrelation between many of the rainfall metrics, the multiple linear regression analysis was used only to select the most predictive independent rainfall variable for final analysis, in addition to water stage variables.

Pore-water pressure

At the index scarp section and time-lapse camera site at WPGC2, four tensiometers (UMS T4e) were used to measure soil pore-water pressure and seepage gradients within a 180-cm scarp profile of an active gully lobe. Tensiometers were situated as pairs at two depths down profile (30 and 105 cm), inserted horizontally (5°) into the scarp face at two distances (40 and 45 cm deep), and backfilled with a slurry of local silt-clay material. Tensiometers were initially installed in January 2010; however, below average wet season rainfall resulted in desiccated subsoils and difficult maintenance conditions. Tensiometers were redeployed during a wetter 20-day period in December 2010. Because of the remote location, tensiometers were only able to be maintained for short durations and were not reinstalled after soil block failure. Available pore-water pressure measurements were graphically compared with measurements and observations of scarp retreat from time-lapse photographs and local rainfall.

RESULTS

Flood frequency across the Mitchell megafan

The magnitude and frequency of flood discharges needed to inundate river inset- and high-floodplains varied longitudinally down the Mitchell fluvial megafan. Along the more incised and confined river and tributary segments of the upper megafan (Figures 1 and 2), gauged flood frequency curves displayed linear trends on a log-probability plot (Figure 4). In contrast, the flood frequency curve at Koolatah (919009A) displayed a nonlinear trend because of the lack of confinement near the Holocene fan apex (Figures 1 and 2). Above the ~2-year RI at Koolatah, there was a progressive loss of water to unmeasured discharge, initially into distributaries at upstream bifurcations and eventually as overbank floodplain discharge (Figure 4).

MODIS satellite imagery (2003–2009) also confirmed the minimum inundation frequency of the Mitchell megafan and lower fandelta, and loss of water from the river channel into distributaries (Figure 5). Comparing the minimum area inundated to the minimum area of active alluvial gullies

DOI: 10.1002/hyp

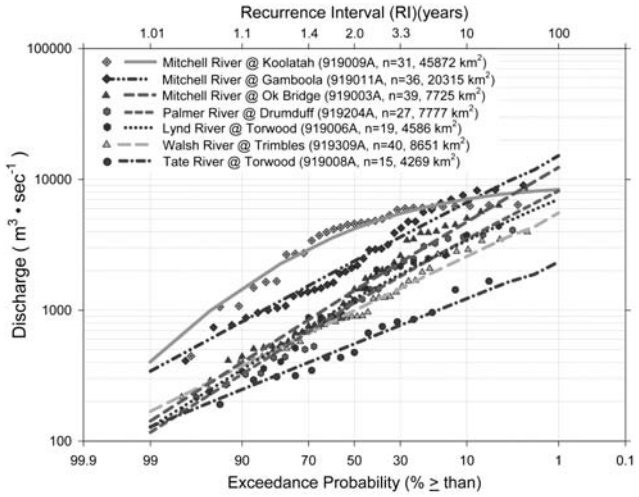

Figure 4. Weibull plotting positions (symbols) and fitted log-Pearson type III flood frequency curves (lines) for discharge gauging sites located in the lower half of the Mitchell catchment [note station ID, sample sizes (n = years) and upstream catchment area].

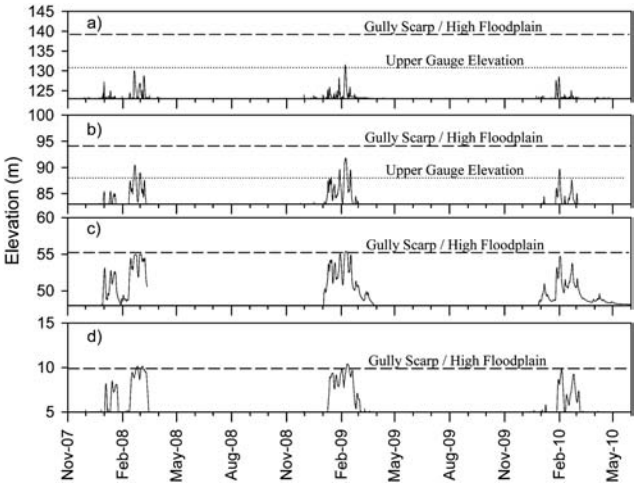

Figure 6. Measured hydrographs of water surface elevation at different alluvial gully sites down the longitudinal profile of the Mitchell megafan: (a) Wrotham Park (WPGC2), (b) Highbury (HBGC1), (c) Onalcal Bar (Onalcal) and (d) Sandy Creek (KWGC2). Long dashed lines represent the elevation of the river high-floodplain surface that local alluvial gullies are eroding into at the gully scarp. The short dashed line represents the elevation of the zero point of the stage gauges nested in the upper alluvial gully-complexes of WPGC2 and HBGC1.

(Brooks *et al*., 2009) suggested that 61% of mapped gullies across the megafan were partially or fully inundated at least once between 2003 and 2009. Only 25% were regularly inundated four or more times, or every 2 years or so, which were concentrated in the Holocene fandelta (Figure 5). Gullies eroding into Pleistocene floodplains of the upper megafan were less frequently inundated, but assessment was difficult because of channel confinement and mixed spectral signals within large pixels.

Flood stage data and hydraulic modelling at study reaches also defined longitudinal increases in floodplain and gully connectivity and flood duration (Figures 6 and 7). At Wrotham Park (WPGC2), the river high-floodplain would only be inundated during stages >100-year RI, whereas flood backwater would partially inundate the gully during events >10-year RI (Figures 7 and 8a). As a consequence of local relief and reduced frequency of flood inundation, the high-floodplain surfaces at Wrotham Park are extensively dissected by alluvial gullies predominantly driven by rainfall–runoff processes (Figure 3a). At Highbury (HBGC1), the river high-floodplain was estimated to be inundated at stages >15-year RI, with flood backwater in the gully measured during 2- to 5-year RI events (Figure 7b). Beyond the 15-year RI at Highbury, floodwater spills over the subtle catchment divide into the Staaten River, reactivating this section of the fluvial megafan (Figure 1; Brooks *et al*, 2009).

At Onalcal Bar, discharge measurements, hydraulic modelling, Koolatah gauge data and MODIS imagery

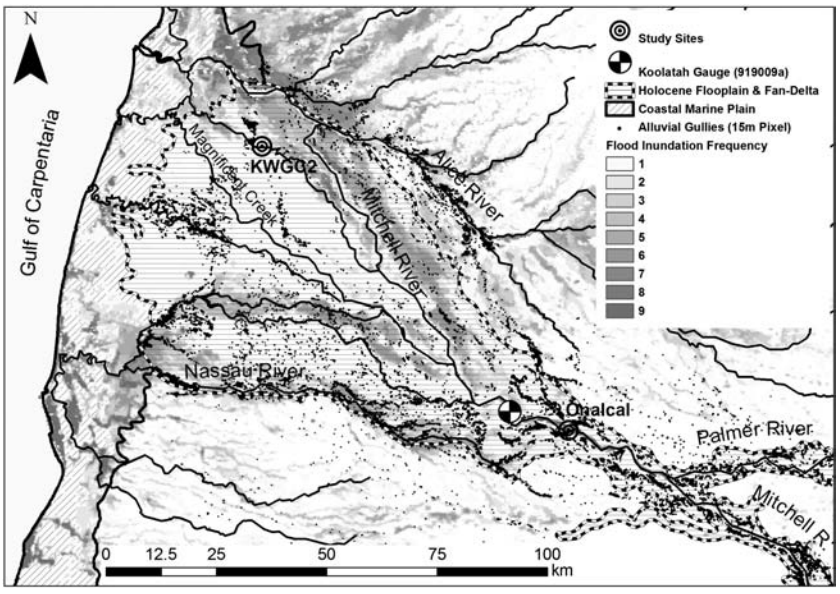

Figure 5. Alluvial gully distribution and flood inundation frequency map of the Mitchell River fandelta. Flood inundation was derived from MODIS (2003–2009) to quantify the number of times inundated. The soil data set from the BRS (1991) highlights the boundary of the active Holocene floodplain and fandelta and coastal plains of the lower Mitchell catchment.

DOI: 10.1002/hyp

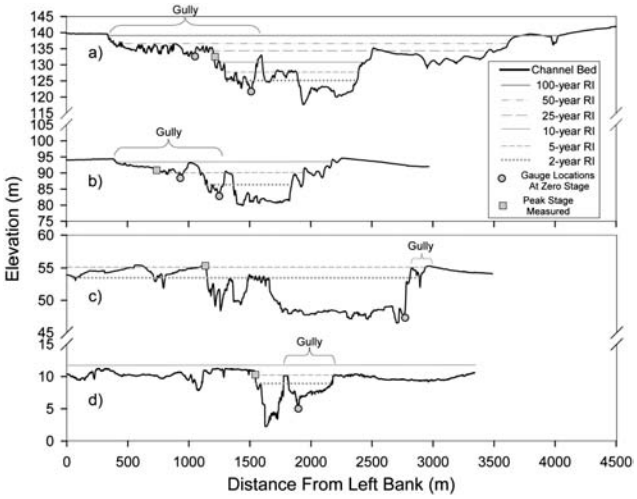

Figure 7. Water surface elevations for different flood frequencies at full river cross sections adjacent to alluvial gully sites down the longitudinal profile of the Mitchell megafan: (a) Wrotham Park (WPGC2), (b) Highbury (HBGC1), (c) Onalcal Bar (Onalcal) (d) Sandy Creek (KWGC2). River cross sections were extracted from LiDAR data at gauge locations within the modelled reach (Figure 3), which also show longitudinal sections of adjacent gullies (not continuous profiles). Zero and peak stage refer to stage data collected between 2007 and 2010 at the specific cross section (Figure 6).

all confirmed that distributaries become increasingly active above the 2-year RI (Figure 7c). Extensive floodplain inundation occurs at or above the 5-year RI, whereas geomorphic units inset within the macrochannel are active during events <2-year RI (Figure 3). Similarly at Sandy Creek (KWGC2), high-frequency overbank flooding and full gully inundation were observed every year during the study period (Figures 5 and 6). Stage correlation with the Koolatah gauge suggested that widespread floodplain inundation from river water occurred at the 5-year RI (Figure 7d). The highest surfaces would be inundated beyond the 7-year RI, which is possibly a result of slight increases in local relative relief in the Mitchell fandelta (Figure 2; Brooks *et al.*, 2009). However, RI results could be influenced by errors inherent in the Koolatah data and correlations over long distances, as compared with local observations of almost annual floodplain inundation from either river water or local rainfall saturation and runoff from smaller drainage networks (Figures 6d and 9; personal communication with Kowanyama Traditional Owners). This inundation and saturation has ramifications for gully scarp retreat rates, as demonstrated below.

Gully area change

Qualitative observations. Daily time-lapse photography demonstrated that annual scarp retreat was the cumulative sum of both subtle and major incremental failures of discrete soil blocks from multiple water sources and erosion mechanisms (Figure 8). Observed water sources for erosion at WPGC2 and HBGC1 came from the combination of direct rainfall, diffuse infiltration-excess water dripping over the scarp face and infiltration-excess runoff plunging off the scarp face during major events. At KWGC2, additional sources came from backwater into and full inundation of the scarp face from river flood water.

Direct rain drop impact gave the appearance of decaying internal gully surfaces in time-lapse because of direct particle displacement, mechanical slaking, physiochemical dispersion and surface wash. Wetting and drying of the scarp face resulted in the spalling of the soil surface from flakes of wetter soil breaking off from the drier material underneath. Linear debris lines of deposited organic material on floodplain surfaces demarcated subtle overland flow paths that resulted in water dripping or plunging off the scarp face at concave lobes (in planform), which were preferential locations of scarp retreat compared with convex interlobes that retreated slower. Infiltration-excess runoff from floodplains following intense rainfall and soil surface sealing was relatively clear compared with turbid runoff below scarp faces from the direct rainfall erosion of exposed subsoils. This indicated that scarps were compressed transition zones between sediment supply- and transport-limited conditions. River backwater and overbank flooding at KWGC2 episodically overwhelmed more typical infiltration-excess runoff processes (Figure 9). River backwater promoted local saturation, soil dispersion and removal of failed soil blocks, steepening the scarp face (Figure 9c). Floodwater drawdown following full inundation created turbulent flow plunging over the scarp face onto saturated soils, enhancing scarp retreat (Figure 9d).

A prerequisite for block failure at active lobes was an over-steepened scarp face undermined by subsoil erosion and dispersion. Erosion of alcoves at the base of scarps was enhanced by the spalling or flaking of surface soils on scarp faces during rainfall wetting and drying, water dripping or plunging off scarp faces, and down-profile changes in soil texture and chemistry (Table II). Tension cracks slowly developed around individual soil blocks and were enhanced by soil wetting and drying, preferential water flow into cracks and changes in pore-water pressure (see below). Undermined scarp blocks often did not fail until subsequent water delivery events surpassed unquantified geotechnical-stability thresholds. Debris slopes of failed soil blocks would temporarily reduce scarp retreat, until the erosion cycle began again with *in situ* breakdown of failed soil blocks and renewed scarp undermining. The presence of trees and their roots near the scarp edge often stalled the advancement of the scarp front along convex interlobes compared with surrounding concave lobes that were more active (in planform). However, active scarp lobes often advanced around trees and their roots, which were eventually undermined by surrounding scarp failure (e.g. Figure 9) or retained on remnant pedestals that slowly eroded *in situ* over time.

Daily quantitative scarp change. The 24-h rainfall total was the best predictor of changes in daily scarp area for all sites (Table III). All other rainfall metrics [NAPI ($k = 0.2$); EI_{30}] were also positively correlated to scarp retreat but were also intercorrelated to 24-h rainfall total (intercorrelation coefficients not shown). The 24-h rainfall was used for final linear correlations (Figure 10), as it is the most direct metric and likely

DOI: 10.1002/hyp

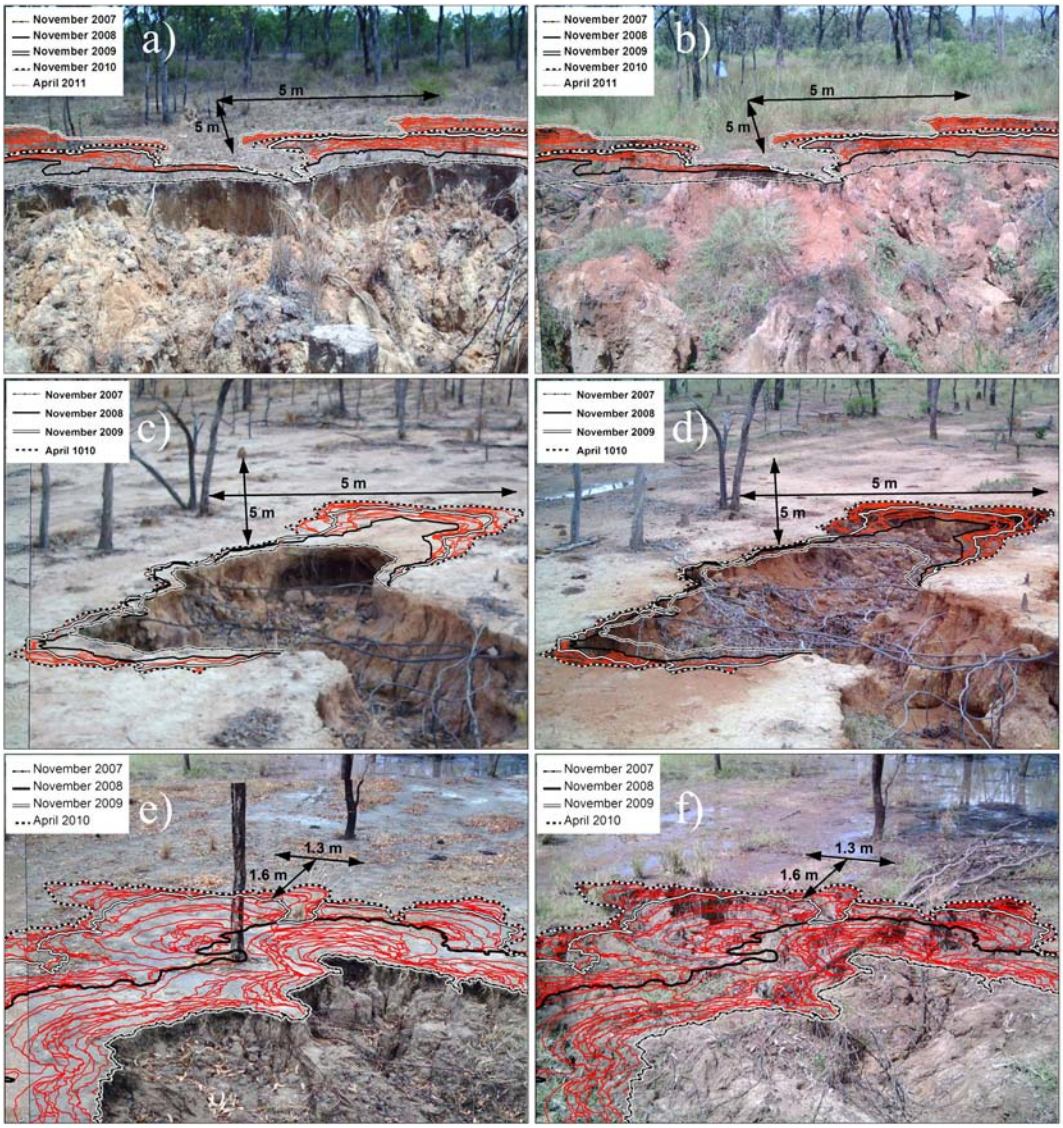

Figure 8. Gully scarp oblique area change at time-lapse camera index sites for (a) WPGC2 on November 2007, (b) WPGC2 on April 2011, (c) HBGC1 on November 2007, (d) HBGC1 on April 2010, (e) KWGC2 on November 2007 and (f) KWGC2 on April 2010. Note that thin (red) lines represent daily incremental changes where measured, as compared with annual scarp locations.

represents a proxy measure for a whole suite of measured and unmeasured variables.

Using rainfall (i.e. 24-h) and stage (i.e. mean daily) metrics in a multiple linear regression only marginally improved erosion prediction at all sites. Stage was a poor predictor of scarp erosion because of the varying incursion of river backwater into gullies unrelated to local rainfall and runoff (Table III). The exception was WPGC2, where maximum stage uninfluenced by backwater was a modest predictive variable. Gauged daily runoff volume at WPGC2 was also highly correlated to scarp retreat (Table III) but also intercorrelated to 24-h rainfall.

At KWGC2, backwater and overbank flooding did not consistently result in increased scarp erosion and weakened correlations between rainfall metrics and scarp retreat when the full data set was used (Table III). A small number of overbank flood days produced most daily area change, whereas others produced much less change (Figure 10c). A subset of data was analysed for only events driven by rainfall–runoff processes without backwater/overbank flooding, which displayed stronger correlations between 24-h rainfall and scarp retreat (Table III; Figure 10c). When river overbank flooding did occur, scarp retreat magnitude often reached high values compared with rainfall or river backwater only (Figure 10c).

For erosion events driven by rainfall and infiltration-excess runoff, linear regressions between 24-h rainfall and scarp area change suggested a threshold of ~10 mm of rainfall needed for initiation of scarp retreat (Figure 10). Beyond this threshold, scarp retreat increased with additional rainfall, but daily rainfall totals still only explained 60% to 70% of the variability in scarp retreat. The remaining variability might be explained by complex intrinsic factors that influence the priming of a scarp face for erosion on a given event, such as antecedent soil moisture and pore-water pressure, cycles of soil block undermining and tension crack development, local heterogeneity in soil properties or preferential surface water flow or drip off the scarp face.

DOI: 10.1002/hyp

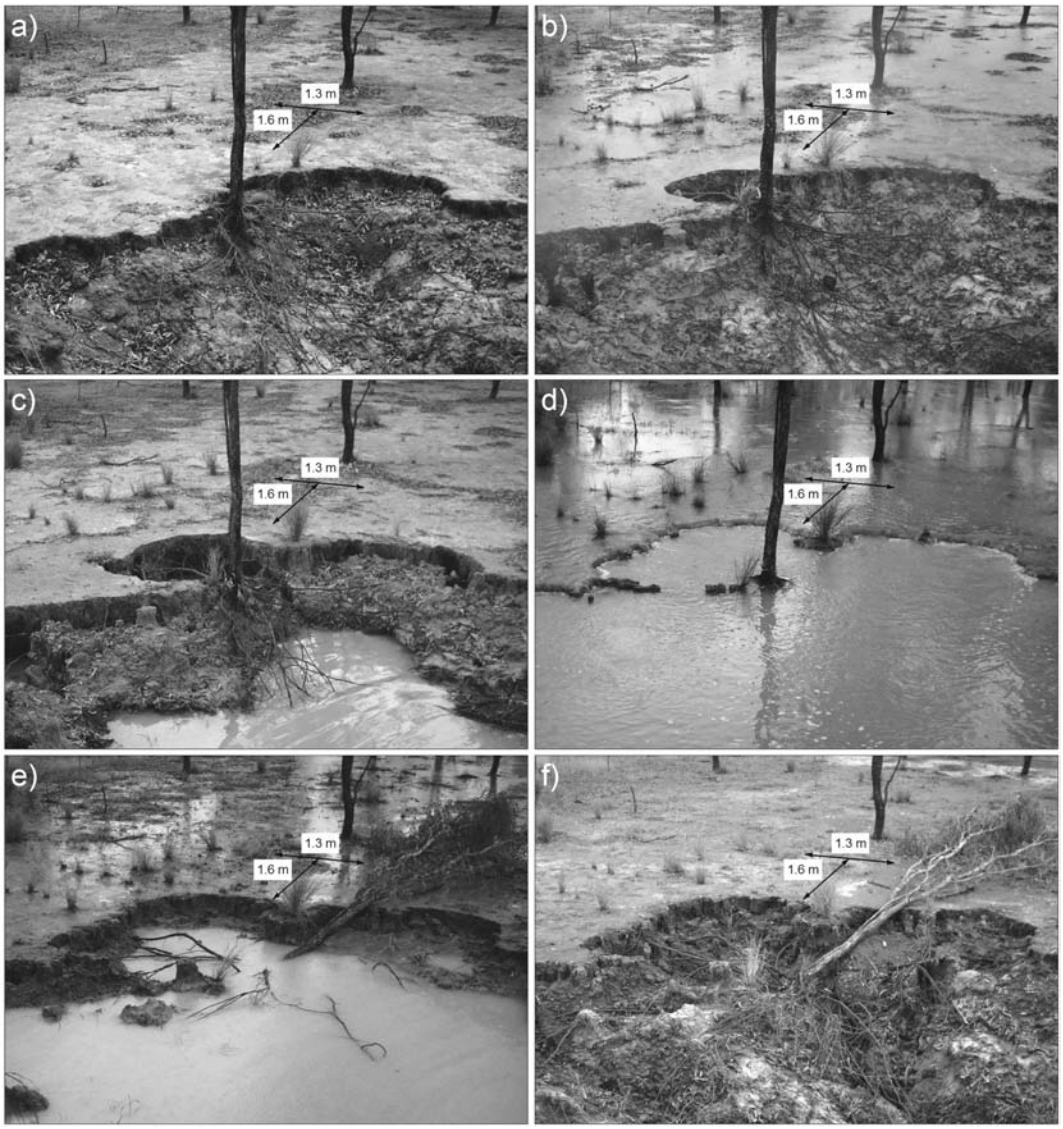

Figure 9. Sequential time-lapse photographs over WY 2009 of an active alluvial gully lobe at the KWGC2 index section in the lower Mitchell River: (a) 28 November 2008, (b) 11 January 2009, (c) 17 January 2009, (d) 01 February 2009, (e) 02 February 2009 and (f) 06 February 2009. Note rainfall induced erosion between panels a and b, backwater and rainfall induced erosion between panels b and c, backwater and overbank-flooding induced erosion between panels c and d and the overland-runoff and flood-drawdown induced erosion between panels d and f.

Additional seasonal differences were also observed between regressions of 24-h rainfall and scarp area change. Early wet season (December and January) regression slopes were significantly different than late wet season slopes (February and March) at WPGC1 ($P < 0.001$, $n = 47$ early, $n = 49$ late, WY 2009–2011) and KWGC2 ($P < 0.001$, $n = 59$ early, $n = 62$ late, WY 2008–2010, rainfall events only). However, slopes were not significantly different for HBGC1 ($P = 0.26$, $n = 52$ early, $n = 47$ late, WY 2009–2010). Although the causation of these seasonal differences is likely multifactorial, the data do hint at the influence of seasonal changes in ground vegetation on water interception, storage and runoff towards gully scarps. Major seasonal changes in grass/weed cover were especially observed at WPGC2 around the gully scarp and contributing surface catchment area (Figures 8a and 8b), with modest cover change at KWGC2 and minimal change at HBGC1 due to scalding and soil surface sealing (Figures 8c and 8d).

Pore-water pressure. During December 2010 at the WPGC2 time-lapse camera index site (Figures 3a and 8a), successful tensiometer measurements of subsurface pore-water pressure were preceded by above average and unseasonably early rainfall in WY 2011 (Figure 11), in contrast to the previous wet season (Table IV). Upper-profile tensiometers (30 cm down, 40–45 cm deep) measured fluctuations in pore-water pressure towards positive values following specific rainfall events and substantial antecedent rainfall (T1 and T2; Figure 11). The event rainfall threshold for initiating a pore pressure response at 30 cm depth was >5 mm but <10 mm and depended largely on antecedent conditions. Lower-profile tensiometers (105 cm down, 40–45 cm deep) did not respond directly to episodic rainfall events but rather measured subtle increases in pore-water pressure as cumulative seasonal rainfall increased (T3 and T4; Figure 11).

At upper-profile tensiometers (30 cm), the time lag between the initiation of rainfall and a pore-water pressure

DOI: 10.1002/hyp

Table III. Pearson correlation coefficients (r) between dependent (daily scarp change) and independent (daily rainfall and water stage) variables

Gully site	No. daily events (n)		Rainfall total (24 h)	Rainfall total (48 h)	Rainfall total (72 h)	I_{30} (daily max)	EI_{30} (daily)	NAPI ($k = 0.8$)	NAPI ($k = 0.2$)	Mean daily stage	Max daily stage	Daily runoff volume
WPGC2	96	Scarp change (m^2)	0.877	0.635	0.511	0.612	0.770	0.563	0.853	0.198	0.420	0.825
HBGC2	97	Scarp change (m^2)	0.774	0.596	0.408	0.611	0.647	0.395	0.747	−0.027	0.082	N/A
KWGC2[a]	188	Scarp change (m^2)	0.370	0.256	0.216	0.310	0.365	0.204	0.344	0.205	0.215	N/A
	(156)		(0.795)	(0.530)	(0.419)	(0.735)	(0.784)	(0.419)	(0.744)			

[a] Values in parentheses are from a subset of days with rainfall only, without river backwater or overbank flow at the scarp zone. N/A, not available.

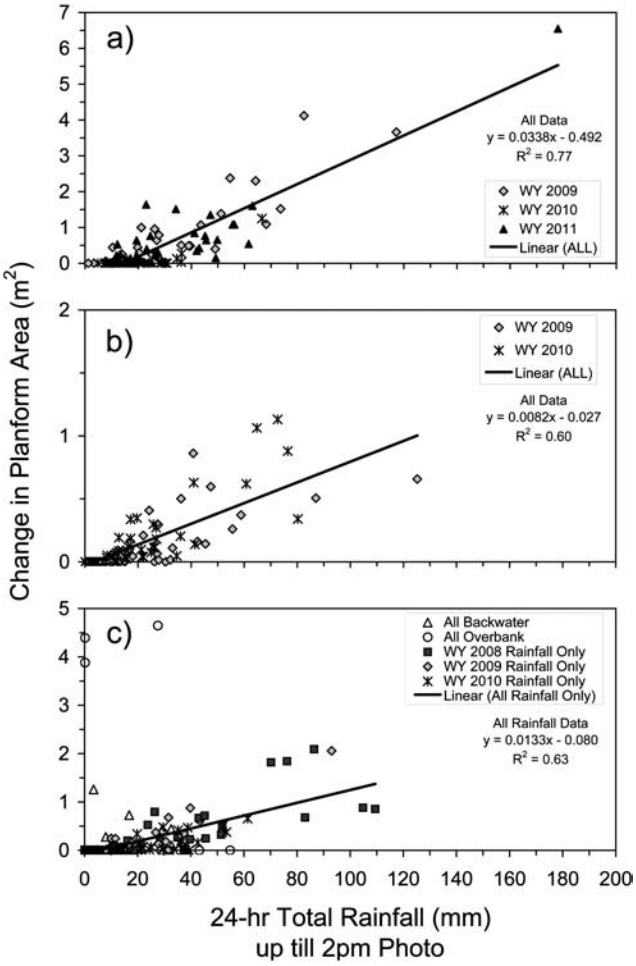

Figure 10. Correlations between estimated daily change in gully planform area (m^2) at index scarp sections (individual lobes) and 24-h total rainfall up till the 2-pm photograph at (a) WPGC2, (b) HBGC1 and (c) KWGC2. Note that erosion due to backwater and overbank flooding at KWGC2 in panel c are included to demonstrate scarp area changes uncorrelated to rainfall.

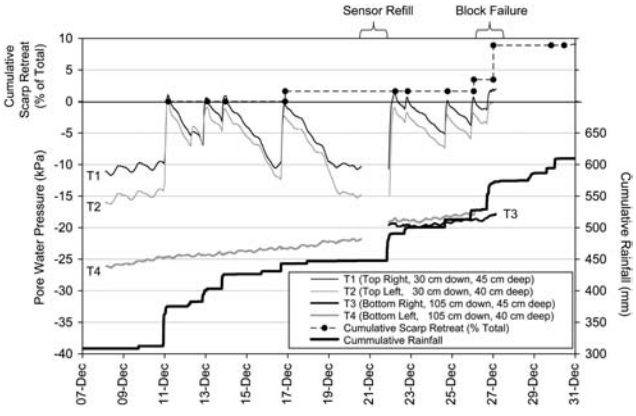

Figure 11. Pore-water pressure (kPa) trends at WPGC2 during WY 2011 from paired tensiometers inserted at two depths down profile (30 and 105 cm) and two distances into the scarp face (40 and 45 cm deep), along with continuous rainfall and scarp retreat at the top edge measured from daily time-lapse cameras.

DOI: 10.1002/hyp

Table IV. Annual erosion measured from time-lapse photos of index scarp sections (individual lobes) in relation to erosion processes and rainfall totals, river backwater and overbank flooding

	Time-lapse camera, scarp index sections				Local rain gauge		GPS surveys for entire gully scarp	
	% Erosion from direct rainfall only (no. days rain >12.7 mm, with no backwater or flooding)	% Erosion from river backwater + rainfall (no. days)	% Erosion from overbank flooding + rainfall (no. days)	% Total change per WY during study period	Annual rainfall (no. days rain >12.7 mm)	Annual rainfall erosivity *R*-factor (no. storms >12.7 mm) (MJ·mm/ha/h/year)	GPS mean scarp retreat rate (length surveyed, m) (m/year)	GPS max scarp retreat rate (m/year)
WPGC2 WY 2008	100% (31 days)	0%[a]	0%	27.9%	1217 mm (31 days)	6507 (27 storms)	0.17 (5507)	4.8
WPGC2 WY 2009	100% (30 days)	0%[a]	0%	34.7%	1235 mm (30 days)	9103 (29 storms)	0.21 (5799)	6.4
WPGC2 WY 2010	100% (15 days)	0%[a]	0%	2.9%	717 mm (15 days)	2841 (14 storms)	0.16 (5762)	1.6
WPGC2 WY 2011	100% (44 days)	0%[a]	0%	34.5%	1884 mm (44 days)	14558 (39 storms)	N/A	N/A
WPGC2 WY 2008–2011	100%	0%[a]	0%	–	Average = 1263 mm	Average = 8252	Average = 0.18	–
HBGC1 WY 2008	100% (33 days)	0%[b]	0%	31.1%	1406 mm (33 days)	9882 (26 storms)	.14 (6260)	3.4
HBGC1 WY 2009	100% (28 days)	0%[b]	0%	41.9%	1303 mm (28 days)	11409 (32 storms)	.10 (6566)	2.4
HBGC1 WY 2010	100% (27 days)	0%[b]	0%	27.0%	1001 mm (27 days)	6077 (26 storms)	.25 (6823)	4.2
HBGC1 WY 2008–2010	100%	0%[b]	0%	–	Average = 1237 mm	Average = 9123	Average = 0.16	–
KWGC2 WY 2008	55.9% (24 days)	6.3% (13 days)	37.8% (8 days)	56.6%	1730 mm (35 days)	14889 (38 storms)	0.14 (2845)	1.6
KWGC2 WY 2009	48.1% (27 days)	14.1% (18 days)	37.8% (6 days)	30.5%	1175 mm (31 days)	7559 (29 storms)	0.11 (2879)	3.1
KWGC2 WY 2010	79.5% (26 days)	3.1% (6 days)	17.4% (1 days)	12.9%	1102 mm (29 days)	7460 (29 storms)	0.17 (2864)	1.6
KWGC2 WY 2008–2010	56.6%	8.3%	35.1%	–	Average = 1336 mm	Average = 9969	Average = 0.14	–

[a] Backwater from river flooding did enter WPGC2 gully floor during all years but only reached 130 m in WY 2008, 131.5 m in WY 2009, 128.5 m in WY 2010 and 131 m in WY 2011, which was >5 m below the elevation of the bottom of the gully scarp (137 m) or >7 m below the top of the gully scarp and river high-floodplain (139.5 m) (Figure 7a).

[b] Backwater from river flooding did enter HBGC1 gully floor during all years but only reached 90.5 m in WY 2008, 91.8 m in WY 2009 and 89.7 m in WY 2010, which was >1 m below the elevation of the bottom of the gully scarp (93.0 m) or >2 m below the top of the gully scarp and river high-floodplain (94.3 m) (Figure 7b).

DOI: 10.1002/hyp

response from displaced antecedent soil water and the wetting front varied inversely with event rainfall magnitude (higher rainfall, quicker response) and antecedent conditions (wetter conditions, quicker response) (median = 0.9 h; max = 4.4 h; min = 0.4 h; $n = 20$). The time lag from the event rainfall centroid to peak pore-water pressure conditions was longer (median = 3.5 h; max = 8.4 h; min = 2.4 h; $n = 20$) and generally increased with rainfall magnitude and event duration. If the latter rates to 30 cm are rough estimates of the saturated hydraulic conductivity of subsoils (median = 85.3 mm/h; max = 126.3 mm/h; min = 35.8 mm/h; $n = 20$), then these rates would exceed observed rainfall intensities during the same events (median = 9.3 mm/h; max = 37.6 mm/h; min = 1.9 mm/h; $n = 20$). However, camera and field observations of soil surface sealing, water ponding and infiltration-excess runoff during large events would suggest that infiltration rates at the immediate soil surface are the limiting factor controlling both deeper infiltration and overland flow generation. More research on infiltration into these sodic, hard-setting soils is needed.

The upper-profile tensiometer located deeper into the scarp face (T1, 45 cm) experienced higher pore-water pressures than the shallower tensiometer (T2, 40 cm), whereas the opposite was true for the lower-profile tensiometers (Figure 11). These data suggest either local soil moisture variability or influence of horizontal wetting and drying fronts and subtle seepage gradients. The continuous matrix suction in the lower-profile and the pressure gradients directed into the scarp face indicate that emergent soil- or groundwater were not driving scarp undercutting and retreat. The development of alcoves at the base of scarp faces was potentially enhanced by the wetting of dispersible, less cohesive subsoils by direct rainfall and runoff over the scarp (Table II), resulting in the spalling of the face as flakes of wetter soil broke off from the drier material underneath. However, in the upper profile, positive pore-water pressures and potential seepage gradients out of the scarp face possibly contributed to reduced shear strength and the failure of small overhanging blocks.

Measurements of local scarp retreat from daily photographs indicated that the failure of overhanging soil blocks was coincident with both rainfall input and increases in upper-profile pore-water pressure. However, only six out of nine events with positive pore-water pressure in the upper-profile resulted in scarp retreat (Figure 11). The measurement period ended when the tensiometers became disturbed from their contact with the soil or were ripped off the scarp face during complete block failure. This occurred during a small rainfall event (16 mm) for a lower-profile tensiometer (T4) and during a larger event (45 mm) for the remaining tensiometers (T1–T3). Complete block failure and major scarp retreat on 27 December 2010 was not associated with major increases in pore-water pressure in the lower profile (T3), whereas upper-profile pressures did reach positive values (T1 and T2; Figure 11).

Annual quantitative change. At the annual scale at WPGC2 and HBGC1, direct rainfall, infiltration-excess runoff and other associated processes dominated erosion at scarps (Table IV). River backwater and overbank flooding could influence erosion during more extreme events (Figures 7a and 7b). In contrast at KWGC2, the total percentage of daily erosion from river backwater (8.3%) and overbank flooding (35.1%) over WY 2008–2010 was considerable, but erosion from just rainfall–runoff events still dominated (56.6%) (Table IV). The contribution of these different processes to scarp erosion varied between years and events. For example, 1 day of overbank flooding in WY 2009 resulted in 10% of the total change in scarp area between WY 2008 and WY 2010 (Figure 9d), whereas 5 days of overbank flooding later in WY 2009 only resulted in 1.3% of the total change.

Average annual rainfall erosivity (R-factor) values from cumulative storms at each site were generally near the 75th percentile value for the region (9456), but with year-to-year variability (Table IV; Yu, 1998; Lu and Yu, 2002). Combining data for all years at all sites but excluding backwater and overbank flooding events, the annual scarp change at index sections was correlated to both annual rainfall erosivity values ($r^2 = 0.75$) and annual rainfall totals ($r^2 = 0.61$) (Table IV).

Mean annual scarp retreat rates measured using GPS across entire scarp fronts were poorly correlated ($r^2 = 0.10$) to measurements of annual rainfall or annual storm erosivity (Table IV). Long lengths of relatively inactive scarp front and horizontal GPS error (± 50 cm) resulted in low signal to noise ratios and overlap of error margins around total gully area change between individual years. Thus, at the annual scale across long lengths of gully front, these GPS data are relatively coarse and are more appropriate for change documentation over multiple years or decades (Shellberg, 2011).

DISCUSSION

Local scarp retreat

The time-lapse photography from nonphotogrammetric digital cameras proved to be practical for quantifying daily scarp retreat and identifying basic geomorphic processes in remote locations. Although not ideal, oblique photos provided useful estimates of relative planform area change. Error inherent in the cameras (Wackrow *et al.*, 2007) or due to oblique distance/scale issues (Chandler *et al.*, 2002) could have partially influenced results. However, the cameras' close proximity to scarps and large relative changes in scarp location likely masked any inherent error. More robust photogrammetric cameras, methods and setups for DEM creation (e.g. Chandler, 1999) could be used in the future, such as vertical views (i.e. towers or trees) or horizontal views of the gully face (Welch *et al.*, 1984; Sneddon *et al.*, 1988; Pyle *et al.*, 1997). Low-altitude large-scale aerial photographs (Marzolff and Poesen, 2009) or high-resolution terrestrial laser scanning (LiDAR) (Heritage and Hetherington, 2007; Resop and Hession, 2010) would be ideal for planform and volumetric change assessment before and after storm events.

DOI: 10.1002/hyp

The correlation of 24-h rainfall totals with daily scarp retreat is suggestive of a cause and effect relationship in the context of intense tropical rainfall impacting, saturating, running off and eroding exposed and dispersible soils. Surprisingly, daily rainfall erosivity (EI_{30}) was not the best predictor of daily scarp retreat despite its integration of multiple storm attributes. However, annual erosivity (*R*-factor) was a better predictor of annual scarp retreat compared with annual rainfall. The variability ($r^2 \approx 0.5$) within rainfall intensity/kinetic energy models used here (Renard *et al*., 1997; Yu, 1998) or elsewhere (van Dijk *et al*., 2002) could be influencing these results, in addition to the lack of empirical rainfall energy data in this part of the wet–dry tropics. Regardless, 24-h rainfall or EI_{30} are just proxy measures for a whole suite of measured and unmeasured variables influencing erosion and scarp retreat. More detailed mechanistic field studies are needed to understand the direct erosion of surface and subsurface soils, internal geotechnical stability and pore-water pressure dynamics, the vegetative influences on water runoff, and the transformation of rainfall and runoff energy into scarp retreat. The mechanistic influence of partial and full floodplain inundation on alluvial gullies along the Mitchell megafan also needs to be investigated in more detail.

Negative pore-water pressures in deeper subsoils during major rainfall and scarp failure events suggest that emergent soil moisture or groundwater seepage out of scarp faces is not dominant or required for scarp failure, in contrast to hypotheses of Brooks *et al*. (2009). The presence of undermined alcoves in subsoils beneath overhanging scarps was misleading as an indicator of water seepage. Alcove features were observed to be enhanced by direct rainfall, spalling or flaking of the scarp face by wetting and drying, and surface water drip and runoff over the scarp face onto less cohesive, sodic subsoils. Evidence for turbulent flow through macropipes was only occasionally observed elsewhere in reconnaissance surveys where pipes followed soil tension cracks, root voids and other soil irregularities and were fed by surface water runoff. However, the lack of evidence for emergent soil moisture or groundwater seepage out of the WPGC2 scarp face does not discount their presence elsewhere. Furthermore, the complete saturation of subsoils during river backwater and overbank flood events at some gullies would undoubtedly create positive pore-water pressures throughout scarp profiles, which would enhance erosion and undercutting during drawdown and subsequent rainfall events (Figures 9 and 10c).

Land use implications

The importance of (i) direct rainfall and infiltration-excess runoff on alluvial gully scarp retreat and (ii) seasonal influences of ground vegetation on water runoff and scarp retreat have implications for grazing land management impacts on soil-surface and grass vegetation conditions. The current land management paradigm of grazing down available grass cover to minimal levels in the late dry season, along with early wet season fire burning of remnant vegetation, results in bare, exposed and disturbed soils at the beginning of the tropical monsoon rains. The sodic, hard-setting, silt/clay soils of the Mitchell floodplains are naturally prone to structural breakdown, surface sealing and enhanced water runoff, which promote gullying. Perennial grass cover as influenced by rangeland management is likely a key factor mitigating this erosion vulnerability and water runoff, through increased rain drop interception, root cohesion, aggregate stability from organic matter, soil permeability and water infiltration (e.g. Bridge *et al*., 1983; McIvor *et al*., 1995; Roth, 2004). Direct soil compaction and destruction of biological crusts by cattle can also influence water infiltration and runoff volumes (Trimble and Mendel, 1995; Evans, 1998). Once runoff occurs, perennial grass cover can increase the resistance of the soil to erosion through root cohesion and surface roughness, which increases the critical shear stress needed for sheet erosion, rilling and gullying (Graf, 1979; Prosser and Slade, 1994; Knapen *et al*., 2007; Knapen and Poesen, 2010). However, cattle tracks can overwhelm vegetative roughness by concentrating overland flow and increasing local shear stress.

In the lower Mitchell catchment, the introduction of cattle in the late 1800s was coincident with the widespread initiation of alluvial gullies into floodplain soils (Shellberg *et al*., 2010; Shellberg, 2011). Reduced vegetative cover and increased physical disturbance of soil by cattle along river banks and near river hollows is hypothesized to have pushed this naturally sensitive landscape across a threshold towards instability. Improved grazing management actions such as riparian fencing and regular maintenance, off-channel water point development and proactive cattle rotation and wet season spelling are needed to reduce soil disturbance, to improve vegetative cover and to reduce the initiation of new gullies into susceptible soils. Furthermore, specific rehabilitation actions need to be locally identified and used to slow or halt alluvial gullies once they have developed into large scarp fronts studied here. More detailed erosion and surface water balance research will be required in connection with experimental gully treatment and control sites to isolate and identify specific cause and effect factors in gully initiation, propagation and stabilization (Shellberg, 2011).

Conceptual model of alluvial gully hydrogeomorphology

Alluvial gullies along floodplain rivers are influenced by a range of hydrogeomorphic processes and are situated within the floodplain perirheic zone or surface water mixing zone (Mertes, 1997). The dominance or mixture of various water sources and erosional processes depends on the vertical and lateral connectivity of the river with adjacent floodplain or gully surfaces, which is displayed in a conceptual model of alluvial gully erosion (Figure 12). This connectivity is temporally dynamic according to the flood pulse concept (Junk *et al*., 1989; Tockner *et al*., 2000), varies spatially and longitudinally along the river continuum and associated process domains (Vannote *et al*., 1980; Montgomery, 1999) and is serially discontinuous because of geomorphic variability (Ward and Stanford, 1995). The locally inherited geomorphic template (e.g. Galloway *et al*., 1970; Grimes and Doutch,

DOI: 10.1002/hyp

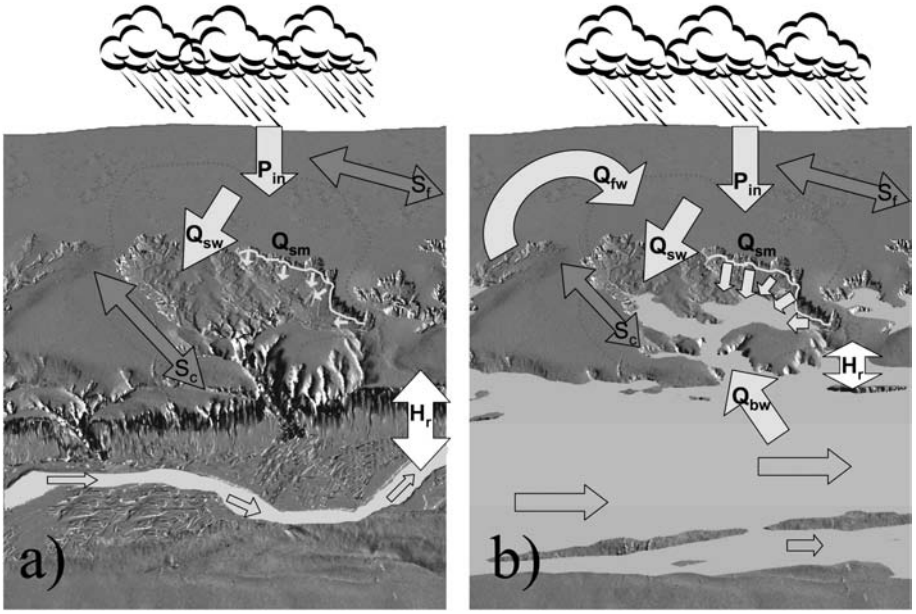

Figure 12. Conceptual model of perirheic-zone erosional drivers of a proximal alluvial gully during: (a) low river water and high relative relief (H_r) when water sources are dominated by direct precipitation (P_{in}), surface water from overland flow off the floodplain (Q_{sw}) and emergent soil moisture (or groundwater) at breaks in slope (Q_{sm}); and (b) high river water and low relative relief (H_r) when water sources additionally include river backwater (Q_{bw}) during common floods and overbank floodplain water (Q_{fw}) during larger magnitude floods. Potential energy factors include relative relief (H_r), alluvial gully channel slope (S_c) and often smaller floodplain slope (S_f). Base image is an oblique LiDAR hillshade of HBGC1 with maximum backwater inundation during the study period in panel b (Figures 6b and 7b).

1978) controls factors such as local relief and topographic slope(s), which are metered by river stage (Figure 12). Climate, geology and land use all control water and sediment supply and the balance of floodplain deposition and erosion (e.g. Ward *et al*., 2011). Resistance to erosion (or lack thereof) is provided by edaphic factors (soil texture, structure, chemistry and pore-water pressure) and vegetative conditions (type, root density, surface cover and soil organic matter). Natural cycles (seasons, drought, flooding and fire) and human land use (cattle grazing, woodland clearing, agriculture, weed invasion and altered fire regimes) can influence vegetative protection and soil disturbance. All of these factors in turn influence the fragile balance of floodplain stability, and whether thresholds are crossed that result in the initiation, propagation and stabilization of alluvial gullies (e.g. Brooks *et al*., 2009; Shellberg, 2011).

The paradox that floodplains can be both sources and sinks of water and sediment is in contrast to conceptual views of floodplains as pure depositional environments (Vannote *et al*., 1980; Junk *et al*., 1989; Montgomery, 1999; Tockner *et al*., 2000). However, the geomorphic position of a floodplain along the (dis)continuum of sediment production, transfer and sink zones in fluvial systems (Schumm 1977; Montgomery 1999) can influence the spatial and temporal scales of sediment storage (e.g. Trimble 1981). It is more appropriate to conceptualize and model floodplain aggradation and degradation as erosion cells (Pickup 1985; 1991) that vary spatially and temporally, especially in relation to gully erosion dynamics (Schumm and Hadley 1957). Small-scale erosion cells (cyclical source, transfer and sinks zones) are typically nested within large-scale fluvial landforms that have similar zones operating at larger and longer time scales. This is the case along the Mitchell River, where new gully erosion cells eroding into Pleistocene alluvium near the top of the megafan (e.g. WPGC2) are net sediment sources to local gully and river inset-floodplains as well as downstream deltaic floodplains or off-shore environments. In contrast, deltaic floodplains that have been sinks of sediment during the Holocene at the landscape scale can still experience local secondary cycles of erosion, as gullies form new erosion cells (e.g. KWGC2) according to local disturbance and changing sediment regimes.

CONCLUSIONS

This research has defined the broad hydrogeomorphic context of the Mitchell megafan in relation to alluvial gully erosion and some locally specific erosional drivers of gully scarp retreat. Land, river and restoration management should be guided by a firm understanding of physical processes acting on large floodplain river systems and influencing different management units important to human and ecological systems. In the lower Mitchell catchment, these management units are best defined from process zones nested at different spatial scales, such as the inherited soils of large-scale fluvial megafan units, the river-segment scale floodplain connectivity and the reach scale dynamics of erosion cell development. Many land management paradigms (e.g. cattle grazing concentrated along waterways), catchment rehabilitation projects (e.g. gully stabilization) or infrastructure development projects (e.g. roads, mines, community infrastructure) are environmentally damaging or ineffective because they do not take these basic hydrogeomorphic forms and processes into account.

DOI: 10.1002/hyp

ACKNOWLEDGEMENTS

Funding was provided by the Australian Government Caring for Our Country program managed by the Northern Gulf Resource Management Group, the Australian Tropical Rivers and Coastal Knowledge (TRaCK) program and Griffith University. Stephen Parker, Vince Manley and others at the Queensland Department of Environment and Resource Management collected and supplied the long-term hydrographic data for the Mitchell catchment. Professor Bofu Yu at Griffith University provided advice and assistance on rainfall erosivity metrics, and Professor Calvin Rose provided valuable comments on early drafts. The managers of Wrotham Park, Highbury and Dunbar Stations and the Kowanyama Aboriginal Land and Natural Resources Management Office graciously provided access to field sites and logistical support. Cultural guidance by Traditional Owners was provided by Vivian Lane for Gugu Mini country around Wrotham/Gamboola and by Willie Banjo for Yir Yoront country around Sandy Creek. Field assistance was provided by the Kowanyama Rangers, Luke and Leon Kingsley, Vivian Lane, Kris Jaeger, Garrett Bean, Carrie Monohan and Ariane Hefferan. Logistical support was provided by Deb Eastop, Brynn Mathews and Bill Sokolich at the Mitchell River Watershed Management Group.

REFERENCES

Australian Bureau of Meteorology (ABOM). 2010. Climate Data. Accessed online in 2010 at: http://www.bom.gov.au/climate/

Brennan S, Gardiner, E. 2004. Geomorphic Assessment of Rivers Series: Gulf Basins and Mitchell Catchment, Queensland Government, Department of Natural Resources and Mines, Technical Report: Brisbane, Australia; 259.

Brice JC. 1966. Erosion and Deposition in the Loess-Mantled Great Plains, Medicine Creek Drainage Basin, Nebraska. U.S. Geological Survey, Professional Paper 352-H: Reston, Virginia; 255–339.

Bridge BJ, Mott JJ, Hartigan RJ. 1983. The formation of degraded areas in the dry savanna woodlands of northern Australia. *Australian Journal of Soil Research* **21**: 91–104. DOI:10.1071/SR9830091

Brooks AP, Spencer J, Shellberg JG, Knight J, Lymburner L. 2008. Using remote sensing to quantify sediment budget components in a large tropical river – Mitchell River, Gulf of Carpentaria. In: Sediment Dynamics in Changing Environments IAHS Publ: Proceedings of a symposium held in Christchurch, New Zealand; December 2008), **325**: 225–236.

Brooks AP, Shellberg JG, Spencer J, Knight J. 2009. Alluvial gully erosion: an example from the Mitchell fluvial megafan, Queensland, Australia. *Earth Surface Processes and Landforms* **34**: 1951–1969. DOI:10.1002/esp.1883. With 2010 Erratum, *Earth Surface Processes and Landforms*, 35: 242–245. DOI:10.1002/esp.1993.

Brunner GW. 2010. HEC-RAS River Analysis System: User Manual Version 4.1, CPD68. U.S. Army Corps of Engineers, Institute for Water Resources, Hydrologic Engineering Center: Davis, California; 790.

Bryan RB, Jones JAA. 1997. The significance of soil piping processes: inventory and prospect. *Geomorphology* **20**: 209–218. DOI:10.1016/S0169-555X(97)00024-X

Bureau of Rural Sciences (BRS). 1991. Digital Atlas of Australian Soils. Originally compiled by K.H. Northcote et al., 1960–68 as the 'Atlas of Australian Soils, Sheets 1 to 10, With Explanatory Data', published by the Commonwealth Scientific and Industrial Research Organisation (CSIRO) and Melbourne University Press: Melbourne, Australia.

Cameron T, Ackerman PE. 2009. HEC-GeoRAS: GIS Tools for the Support of HEC-RAS Using ArcGIS, Version 4.2, CPD83. U.S. Army Corps of Engineers, Institute for Water Resources, Hydrologic Engineering Center: Davis, California; 246.

Chandler J. 1999. Effective application of automated digital photogrammetry for geomorphological research. *Earth Surface Processes and Landforms* **24**: 51–63. DOI:10.1002/(SICI)1096-9837(199901)24:1<51::AID-ESP948>3.0.CO;2-H

Chandler, J, Ashmore, P, Paola, C, Gooch, M, Varkaris, F. 2002. Monitoring river-channel change using terrestrial oblique digital imagery and automated digital photogrammetry. *Annals of the Association of American Geographers* **92**: 631–644. DOI:10.1111/1467-8306.00308.

Chow VT. 1959. Open Channel Hydraulics. McGraw Hill: New York; 680.

Condon RW. 1986. A Reconnaissance Erosion Survey of part of the Victoria River District, N.T.. Hassall & Associates: Canberra, Australia; 284.

Cudworth AG Jr.. 1989. Flood Hydrology Manual. United States Department of the Interior, Bureau of Reclamation, Surface Water Branch, Earth Sciences Division, Water Resources Technical Publication: Denver, CO; 243.

DeVries JJ. 1976. The groundwater outcrop-erosion model: evolution of the stream network in the Netherlands. *Journal of Hydrology* **29**: 43–50. DOI:10.1016/0022-1694(76)90004-4.

Dunne T, Black RD. 1970. Partial area contributions to storm runoff in a small New England watershed. *Water Resources Research* **6**: 1296–1311. DOI:10.1029/WR006i005p01296.

Evans R. 1998. The erosional impacts of grazing animals. *Progress in Physical Geography* **22**: 251–268. DOI:10.1177/030913339802200206.

Galloway RW, Gunn RH, Story R. 1970. Lands of the Mitchell-Normanby Area, Queensland. CSIRO, Land Research Series No 26; 101.

Goudie AS. 1973. Duricrusts in Tropical and Subtropical Landscapes. Clarendon Press: Oxford; 174.

Graf WL. 1979. The development of montane arroyos and gullies. *Earth Surface Processes* **4**: 1–14. DOI:10.1002/esp.3290040102.

Grimes KG, Doutch HF. 1978. The late Cainozoic evolution of the Carpentaria Plains, Northern Queensland. *BMR Journal of Australian Geology and Geophysics* **3**: 101–112.

Haigh MJ. 1998. Ravine erosion and reclamation in India. In: Managing Agriculture for a Better Tomorrow: The Indian Experience, DC Pandey (Ed.) MD Publications PVT LTD: New Delhi; 161–193.

Heggen RJ. 2001. Normalized antecedent precipitation index. *Journal of Hydrologic Engineering* **6**: 377–381. DOI:10.1061/(ASCE)1084-0699(2001)6:5(377).

Heritage G, Hetherington D. 2007. Towards a protocol for laser scanning in fluvial geomorphology. *Earth Surface Processes and Landforms* **32**: 66–74. DOI:10.1002/esp.1375.

Horton, RE. 1933. The role of infiltration in the hydrologic cycle. *EOS, Transactions, American Geophysical Union* **14**: 446–460.

Junk WJ, Bayley PB, Sparks RE. 1989. The flood pulse concept in river-floodplain systems. In: Proceedings of the International Large River Symposium, Dodge DP (Ed). Canadian Special Publication of Fisheries and Aquatic Sciences **106**: 110–127.

Kirkby MJ, Chorley RJ. 1967. Throughflow, overland flow and erosion. *Bulletin of the International Association of Scientific Hydrology* **12**: 5–21. DOI:10.1080/02626666709493533.

Kirkby M. 1988. Hillslope runoff processes and models. *Journal of Hydrology* **100**: 315–339. DOI:10.1016/0022-1694(88)90190-4.

Knapen A, Poesen J, Govers G, Gyssels G, Nachtergaele J. 2007. Resistance of soils to concentrated flow erosion: a review. *Earth-Science Reviews* **80**: 75–109. DOI:10.1016/j.earscirev.2006.08.001.

Knapen A, Poesen, J. 2010. Soil erosion resistance effects on rill and gully initiation points and dimensions. *Earth Surface Processes and Landforms* **35**: 217–228. DOI:10.1002/esp.1911.

Lu H, Yu B. 2002. Spatial and seasonal distribution of rainfall erosivity in Australia. *Australian Journal of Soil Research* **40**: 887–901. DOI:10.1071/SR01117.

Marzolff I, Poesen J. 2009. The potential of 3D gully monitoring with GIS using high-resolution aerial photography and a digital photogrammetry system. *Geomorphology* **111**: 48–60. DOI:10.1016/j.geomorph.2008.05.047.

McCloskey GL. 2010. Riparian Erosion Morphology, Processes and Causes along the Victoria River, Northern Territory, Australia. Charles Darwin University, PhD Thesis; 200.

McIvor JG, Williams J, Gardener CJ. 1995. Pasture management influences runoff and soil movement in the semi-arid tropics. *Australian Journal of Experimental Agriculture* **35**: 55–65. DOI:10.1071/EA9950055.

McTainsh GH, Lynch AW, Hales R. 1997. Particle-size analysis of aeolian dusts, soils and sediments in very small quantities using a Coulter multisizer. *Earth Surface Processes and Landforms* **22**: 1207–1216. DOI:10.1002/(SICI)1096-9837(199724)22:13<1207::AID-ESP820>3.0.CO;2-K.

Mertes LAK. 1997. Documentation and significance of the perirheic zone on inundated floodplains. *Water Resources Research* **33**: 1749–1762. DOI:10.1029/97WR00658.

Mertes LAK, Dunne T. 2008. Effects of tectonism, climate change, and sea-level change on the form and behaviour of the modern Amazon river

and its floodplain. In: Large Rivers: Geomorphology and Management, A Gupta (Ed.) John Wiley and Sons: West Sussex, UK; 115–144.

Montgomery DR. 1999. Process domains and the river continuum. *Journal of the American Water Resources Association* **35**: 397–408. DOI: 10.1111/j.1752-1688.1999.tb03598.x.

Naidu R, Sumner ME, Rengasamy P. 1995. Australian sodic soils: distribution, properties, and management. CSIRO Publications: East Melbourne, Victoria, Australia; 351.

Nott J, Haig J, Neil H, Gillieson D. 2007. Greater frequency variability of landfalling tropical cyclones at centennial compared to seasonal and decadal scales. *Earth and Planetary Science Letters* **255**: 367–372. DOI: 10.1016/j.epsl.2006.12.023.

Oostwoud Wijdenes D, Poesen J, Vandekerckhove L, Ghesquiere M. 2000. Spatial distribution of gully head activity and sediment supply along an ephemeral channel in a Mediterranean environment. *Catena* **39**: 147–167. DOI:10.1016/S0341-8162(99)00092-2.

Oostwoud Wijdenes D, Bryan R. 2001. Gully-head erosion processes on a semi-arid valley floor in Kenya: A case study into temporal variation and sediment budgeting. *Earth Surface Processes and Landforms* **26**: 911–933. DOI:10.1002/esp.225.

Pain, CF, Ollier, CD. 1992. Ferricrete in Cape York Peninsula, Northern Queensland. *BMR Journal of Australian Geology and Geophysics* **13**: 207–212.

Parker G, Muto T, Akamatsu Y, Dietrich WE, Lauer JW. 2008. Unravelling the conundrum of river response to rising sea-level from laboratory to field. Part II. The Fly–Strickland River system, Papua New Guinea. *Sedimentology* **55**: 1657–1686. DOI:10.1111/j.1365-3091.2008.00962.

Pickup G. 1985. The erosion cell: a geomorphic approach to landscape classification in range assessment. *Australian Rangeland Journal* **7**: 114–121. DOI:10.1071/RJ9850114.

Pickup G. 1991. Event frequency and landscape stability on the floodplain systems of arid Central Australia. *Quaternary Science Reviews* **10**: 463–473. DOI:10.1016/0277-3791(91)90007-H.

Piest RF, Bradford JM, Wyatt GM. 1975. Soil erosion and sediment transport from gullies. *Journal of the Hydraulics Division, Proceedings of the American Society of Civil Engineers* **101**: 65–80.

Poesen J. 1993. Gully typology and gully control measures in the European loess belt. In: Farm Land Erosion in Temperate Plains Environment and Hills, S Wicherek (Ed). International Symposium on Farm Land Erosion: Paris France, 25–29 May 1992, Elsevier Amsterdam; 221–239.

Poole GC. 2002. Fluvial landscape ecology: addressing uniqueness within the river discontinuum. *Freshwater Biology* **47**: 641–660. DOI:10.1046/j.1365-2427.2002.00922.x.

Pringle HJR, Watson IW, Tinley KL. 2006. Landscape improvement, or ongoing degradation – reconciling apparent contradictions from the rangelands of Western Australia. *Landscape Ecology* **21**: 1267–1279. DOI:10.1007/s10980-006-0015-x.

Prosser IP, Slade CJ. 1994. Gully formation and the role of valley-floor vegetation, southeastern Australia. *Geology* **22**: 1127–1130. DOI:10.1130/0091-7613(1994)022<1127:GFATRO>2.3.CO;2

Pyle CJ, Richards KS, Chandler JH. 1997. Digital photogrammetric monitoring of river bank erosion. *The Photogrammetric Record* **15**: 753–764. DOI:10.1111/0031-868X.00083.

Queensland Department of Environment and Resource Management (QDERM). 2010. Hydrographic Gauge Data. Provided by the State of Queensland, 2010.

Rayment GE, Higginson FR. 1992. Australian Laboratory Handbook of Soil and Water Chemical Methods. Inkata Press: Melbourne; 330.

Renard KG, Foster GR, Weesies GA, McCool DK, Yoder DC. 1997. Predicting Soil Erosion By Water: A Guide to Conservation Planning with the Revised Universal Soil Loss Equation (RUSLE). US Department of Agriculture, Agricultural Handbook 703: Washington, DC; 404.

Resop, JP, Hession WC. 2010. Terrestrial laser scanning for monitoring streambank retreat: comparison with traditional surveying techniques. *Journal of Hydraulic Engineering ASCE* **136**: 794–798. DOI:10.1061/(ASCE)HY.1943-7900.0000233.

Roth CH. 2004. A framework relating soil surface condition to infiltration and sediment and nutrient mobilization in grazed rangelands of northeastern Queensland, Australia. *Earth Surface Processes and Landforms* **29**: 1093–1104. DOI: 10.1002/esp.1104.

Schumm SA, Hadley RF. 1957. Arroyos and the semiarid cycle of erosion. *American Journal of Science* **255**: 161–74.

Schumm SA. 1977. The Fluvial System. Wiley: New York.

Sharma HS. 1987. Morphology and origin of ravines. In: Tropical geomorphology: a morphogenetic study of Rajasthan. HS Sharma (Ed). Naurang Rai Concept Publishing Company: New Delhi; 229–251.

Shellberg J, Brooks A, Spencer J. 2010. Land-use change from indigenous management to cattle grazing initiates the gullying of alluvial soils in northern Australia, *19th World Congress of Soil Science, Soil Solutions for a Changing World*. (1–6 August 2010), Brisbane, Australia; 59–62.

Shellberg JG. 2011. Alluvial Gully Erosion Rates and Processes Across the Mitchell River Fluvial Megafan in Northern Queensland, Australia. Griffith University, PhD Thesis, Brisbane, Australia; 257.

Simpson CJ, Doutch HF. 1977. The 1974 wet-season flooding of the southern Carpentaria Plains, northwest Queensland. *BMR Journal of Australian Geology and Geophysics* **2**: 43–51.

Singh S, Dubey A. 2000. Temporal variations in the network of man-impacted gully basins in the sub-humid tropical alluvial riverine environment - A case study of Deoghat gullies of Allahabad District, India. *Zeitschrift für Geomorphologie* **44**: 175–194.

Sneddon J, Williams BG, Savage JV, Newman CT. 1988. Erosion of a gully in duplex soils: Results of a long-term photogrammetric monitoring program. *Australian Journal of Soil Research* **26**: 401–408. DOI:10.1071/SR9880401.

Stewart BJ. 1993. The hydrology and water resources of humid northern Australia and Papua New Guinea. In: Hydrology and Water Management in the Humid Tropics: Hydrological Research Issues and Strategies for Water Management. M Bonell, MM Hufschmidt and JS Gladwell (Eds). Cambridge University Press: International Hydrology Series; 67–83.

Thomas JT, Iverson NR, Burkart MR, Kramer LA. 2004. Long-term growth of a valley-bottom gully, western Iowa. *Earth Surface Processes and Landforms* **29**: 995–1009. DOI: 10.1002/esp.1084.

Tockner K, Malard F, Ward JV. 2000. An extension of the flood pulse concept. *Hydrological Processes* **14**: 2861–2883. DOI:10.1002/1099-1085(200011/12)14:16/17<2861::AID-HYP124>3.0.CO;2-F.

Tothill JC, Nix HA, Stanton JP, Russell MJ. 1985. Land use and productive potentials of Australian savanna lands. In: Ecology and Management of the World's Savannas. JC Tothill, JJ Mott (Eds). Australian Academy of Science: Canberra, ACT; 125–141.

Trimble SW. 1981. Changes in sediment storage in the Coon Creek Basin, Driftless Area, Wisconsin, 1853 to 1975. *Science* **214**: 181–183.

Trimble SW, Mendel AC. 1995. The cow as a geomorphic agent: a critical review. *Geomorphology* **13**: 233–253. DOI:10.1016/0169-555X(95)00028-4.

U.S. Water Resources Council (USWRC). 1981. Guidelines for Determining Flood Flow Frequency. U.S. Water Resources Council: Bulletin 17B; 194.

van Dijk AIJM, Bruijnzeel LA, Rosewell CJ. 2002. Rainfall intensity - kinetic energy relationships: a critical literature appraisal. *Journal of Hydrology* **261**: 1–23. DOI:10.1016/S0022-1694(02)00020-3.

Vandekerckhove L, Poesen J, Oostwoud Wijdenes D, Gyssels G, Beuselinck L, de Luna E. 2000. Characteristics and controlling factors of bank gullies in two semi-arid Mediterranean environments. *Geomorphology* **33**: 37–58. DOI:10.1016/S0169-555X(99)00109-9.

Vandekerckhove L, Gyssels G, Poesen J, Oostwoud Wijdenes D. 2001. Short-term bank gully retreat rates in Mediterranean environments. *Catena* **44**: 133–161. DOI:10.1016/S0341-8162(00)00152-1.

Vandekerckhove L, Poesen J, Govers G. 2003. Medium-term gully headcut retreat rates in southeast Spain determined from aerial photographs and ground measurements. *Catena* **50**: 329–352. DOI:10.1016/S0341-8162(02)00132-7.

Vannote RL, Minsall GW, Cummins KW, Sedell JR, Cushing CE. 1980. The river continuum concept. *Canadian Journal of Fisheries and AquaticScience* **37**: 103–137. DOI: 10.1139/f80-017.

Wackrow R, Chandler JH, Bryan P. 2007. Geometric consistency and stability of consumer-grade digital cameras for accurate spatial measurement. *The Photogrammetric Record* **22**: 121–134. DOI: 10.1111/j.1477-9730.2007.00436.x.

Ward JV, Stanford JA. 1995. The serial discontinuity concept: extending the model to floodplain rivers. *Regulated Rivers: Research & Management* **10**: 159–168. DOI: 10.1002/rrr.3450100211.

Ward D, Brooks A, Pusey B, Olley J, Shellberg J, Spencer J, Knight J. 2011. Riverine landscapes and aquatic system diversity. In: Aquatic biodiversity in northern Australia: patterns, threats and future. B Pusey (Ed). Charles Darwin University Press: Darwin, N.T., Australia; 5–22.

Ward D, Hamilton S, Jardine T, Pettit N, Tews K, Olley J, Bunn S. 2012 accepted. Assessing the seasonal dynamics of inundation, turbidity and aquatic vegetation in the Australian wet–dry tropics using optical remote sensing. *Ecohydrology*.

Welch R, Jordan TR, Thomas AW. 1984. A photogrammetric technique for measuring soil erosion. *Journal of Soil and Water Conservation* **39**: 191–194.

Yadav RC, Bhushan LS. 2002. Conservation of gullies in susceptible riparian areas of alluvial soil regions. *Land Degradation and Development* **13**: 201–219. DOI: 10.1002/ldr.493.

Yu B. 1998. Rainfall erosivity and its estimation for Australia's tropics. *Australian Journal of Soil Research* **36**: 143–165. DOI:10.1071/S97025.